No general circulation of the atmosphere without cyclones
is dynamically possible when friction is taken into account

Jeffreys, 1926

Chapter 6
Momentum ~~and Static Energy~~

Purpose: This chapter tracks momentum ~~and static energy~~ in the atmosphere. The general circulation is foremost about motion. So, this chapter initiates the discussion of maintenance and tendency in the motion. This chapter examines momentum more deeply than in Chapter 1. Maintaining momentum is not a detail, but a key factor in determining the structure of Earth's general circulation. In middle latitudes transient eddy fluxes dominate maintaining westerly momemtum broadly and even so-called "eddy-driven" jets; but not the climatological subtropical jet stream. That subtropical jet is linked to mean meridional overturning through the Coriolis term. However, motions are linked to temperature through pressure forces and the interaction between heat and momentum is captured by analyzing energetics; those discussions are reserved for the next chapter.

~~Heat flux was invoked for radiative balance and temperature discussions in Chapter 3, those fluxes arise here in the context of atmospheric energy.~~

~~The etc. <<< abstract >>> Before discussing energetics in detail, Also discussed are dry and moist static energies (DSE and MSE, respectively). And some global views of energetics beyond those seen in Chapter 3.~~

6.1 Angular Momentum and Its Maintenance

6.1.1 Angular momentum and angular velocity

Our starting point is to examine the absolute angular momentum $\mathscr{M}$ of an air parcel. There are two reasons. First $\mathscr{M}$ is conserved unless torques are applied to the parcel. Second, equations for $\mathscr{M}$ link the atmosphere's gross dynamics to those of the oceans and solid Earth. Three important forces for the atmosphere are gravity, pressure force, and friction. These forces

can create torques that may change the atmospheric angular momentum (AAM). When a parcel is moving, the momentum of its motion also includes the motion of the coordinate frame fixed with respect to the rotating Earth. Egger et al. (2007) have a more extensive review of the momentum balance including discussion of the central role of AAM in the general circulation.

Technically, $\mathscr{M}$ has three components and traditionally, all point outwards from the Earth's center. Two point outward through the equator (typically at 0 and 90 E). The third points outward through the North Pole and is labeled the "axial component". The axial component is interchangeably labelled the "zonal component" here since only the zonal component of the wind contributes to it. For the other AAM components, meridional and zonal winds can contribute. These latter two components are sometimes called the *equatorial AAM vector*. Motions, particularly in the tropics can impact the two non-axial components. Major polar topography (Antarctica and Greenland) are particularly important (Feldstein, 2006) forcing of equatorial AAM vector phase and amplitude variations. However, the purposes of this discussion are adequately served by focusing on the axial component of the AAM. Only the axial component of $\mathscr{M}$ is considered here. That is effectively the component about the axis of Earth's rotation. The other two components are much smaller. $\mathscr{M}$ has contributions from Earth's rotation (labelled the "planetary" part) and from atmospheric winds (labelled the "wind" part). The planetary part of the axial component is three to four orders of magnitude larger than the other two planetary components. Similarly, the 'wind' part of the axial component is about 50 times larger than the corresponding other two components (Egger et al., 2007). Even if the atmosphere is at rest with respect to the Earth's surface, it has angular momentum expressed by the "planetary" angular velocity term due to the Earth's rotation. If the air parcel changes latitude, even when staying on a constant geopotential surface, then the parcel's distance from the axis of rotation ($= r\cos\varphi$) changes and this effect must be included in our equations. Figure 6.1 shows the geometry.

Aside from neglecting the other components, the atmosphere is assumed to be thin enough so that changes in the distance from the axis of rotation due to vertical motions are neglected. Also neglected is a "moisture torque" from the cycle of atmospheric water vapor (Egger, 2006). Finally, the Earth is assumed to be a sphere.

The symbol M designates the absolute angular *velocity* of a parcel. As noted, M has two parts because the coordinate system is fixed with respect to the earth and thus rotates.

$$M = R_c^2\,\Omega + R_c\,u \tag{6.1}$$

where

$$R_c = r \cos\phi$$

The first part is the planetary angular velocity while the second part is the velocity relative to the rotating coordinate system. The earth's radius is r and ϕ is latitude; Ω is the angular speed of the Earth's rotation; and u is zonal velocity (positive in the direction of earth's motion). Appendix B has a complete list of variable designations.

Angular momentum $\mathcal{M}$ equals ρM. Because density enters into the AAM, the budget for the stratosphere is small. On a time mean, the primary features are the jet streams (with $\mathcal{M}$ maximum at lower elevation than the zonal wind max, e.g. Figure 4.13, due to the density weighting) and low level motions. While important for overall balance, the torques applied at the Earth's surface are notable only in the lower half of the troposphere (Egger et al., 2007) whereas the upper troposphere and stratosphere momentum are dominated by transports by MMCs and eddies.

6.1.2 Angular Momentum Tendency

The annual cycle is the largest contributor to variability of the AAM (Kang and Lau, 1994) with nearly 4/5 of that variability due to seasonal variation of the jet streams. Global AAM is largest in mid-November and mid-April and least at the start of August (Egger et al., 2007). Other variability is associated with low frequency phenomena such as: ENSO (e.g. Black et al., 1996), QBO (Chao, 1989), and MJO (e.g. Weickmann et al., 1997).

The rate of change of angular momentum depends on pressure forces along the zonal direction and friction acting on motion along that same direction.

$$\rho \frac{dM}{dt} + R_c \frac{\partial P}{\partial x} + R_c F_x = 0 \qquad (6.2)$$

ρ is density, $\partial P/\partial x$ is the pressure gradient in the longitudinal dimension, and F_x is friction in the longitudinal direction x (defined with the same sign as M). One can derive a spherical coordinates form of this relationship (e,g, Ionescu-Kruse, 2022) but only a general insight is desired at this point. Similarly, the pressure gradient term above is simplified because the *mechanical* pressure in compressible fluids can differ from the *thermodynamic* pressure, p (White, 2006). The difference may be approximated by Stokes' (1845) hypothesis. However, to avoid developing the greater complexity at the expense of clarity, Cartesian coordinates and

thermodynamic pressure are used here. Equation (6.2) is easily derived from the zonal velocity equation (e.g. C.26 in Appendix C); the Coriolis term is within the $v\,\partial M/\partial y$ term.

Expanding the total derivative in (6.2) yields:

$$\frac{\partial(\rho M)}{\partial t}+\nabla_3\cdot\rho M\mathbf{V}_3+R_c\frac{\partial P}{\partial x}+R_c F_x=0 \tag{6.3}$$

Integrating (6.3) over the volume of the atmosphere between latitude circles ϕ_1 and ϕ_2 while holding volume V constant obtains:

$$\frac{\partial}{\partial t}\int_V \rho M\,dV=\int_{S_1}\rho M v_1\,dxdz-\int_{S_2}\rho M v_2\,dxdz-\int_V R_c\frac{\partial P}{dx}dV-\int_V R_c F_x dV \tag{6.4}$$

Here S_1 equals the surface area of the "wall" at latitude circle ϕ_1; S_2 equals the surface area of the "wall" at latitude circle ϕ_2; and v_i equals meridional velocity directed positive into ϕ_i from the south.

Figure 6.2 illustrates the orientation. The only surface integrals obtained in (6.4) are those along the meridional boundary "walls." No contribution comes from the longitudinal direction because the domain encircles the earth, i.e., because of the periodic boundary condition. While obstructions cause a non-zero contribution for the pressure gradient term, they cannot do so for the zonal velocity gradient term. Finally, the top and bottom boundaries make no contribution because the vertical velocity vanishes there.

The time derivative term is approximately zero when averaged over a year's time. The time derivative can be ignored when dealing with long period problems of the general circulation. For a long-term average the friction term is cumulative and eventually becomes a large accumulation. Over the short term, the time derivative must be included but the friction term can be dropped.

The first three terms on the right-hand side of (6.4) are responsible for bringing angular momentum in (or out) of the volume. Both of the first two right-hand side terms in (6.4) can be rewritten. For example, by applying a time average to the first term and using the hydrostatic equation to make a change of independent variable, one obtains:

$$\int_{S_1}\int_t \rho M v_1\,dxdzdt=\frac{R_c{}^2\Omega}{g}\int_0^{P_0}\int_x\int_t v_1\,dtdxdP+\frac{R_c}{g}\int_0^{P_0}\int_x\int_t uv_1\,dtdxdP \tag{6.5}$$

The flux has been split into two parts. One part is advection of planetary angular momentum (which includes a mass flux across the latitude circle). Using the shorthand notation developed in

Appendix A and applying it to both surface integrals, then one can write the first two terms on the RHS of (6.4):

$$\underbrace{\frac{R_{c1}{}^2\Omega L\tau P_0}{g}\overbrace{[v_1]}-\frac{R_{c2}{}^2\Omega L\tau P_0}{g}\overbrace{[v_2]}}_{(A)}+\underbrace{\frac{R_{c1}L\tau P_0}{g}\overbrace{[u_1v_1]}-\frac{R_{c2}L\tau P_0}{g}\overbrace{[u_2v_2]}}_{(B)} \tag{6.6}$$

In (6.6) subscripts have been added to R_c and u to make clear that these quantities are likely to be different at the two latitude 'walls'.

- *Term (A)* transfers *planetary* angular momentum through a net mass shift into or out of the volume, across latitudes ϕ_1 and ϕ_2. If the transfer is towards the closer pole (South or North) then the term is positive as the *net* motion is towards a location a shorter distance from the axis of rotation. For example, in the Southern Hemisphere, a net shift towards the South Pole has $R_{c1} < R_{c2}$ but the meridional velocities are negative leaving term *(A)* positive.
- *Term (B)* is a northward flux of *relative* angular momentum that can be split into terms associated with simple categories of circulations (discussed in Appendix A). Again, the sign of the term depends on the *net* transfer into or out of the volume. For example, in the Northern Hemisphere, if $R_{c1}\overbrace{[u_1v_1]}>R_{c2}\overbrace{[u_2v_2]}$ then there is a *net* convergence of relative angular momentum in the volume.

The third term on the right-hand side of equation (6.4) is the pressure or "orographic" or "mountain" torque term. As discussed in Chapter 1, if the zonal integral goes completely around the earth, then

$$\int\frac{\partial P}{\partial x}dx=0$$

and the term vanishes. However, if a mountain obstructs the circuit, then the integral takes the form:

$$\int\int R_c(P_2-P_1)dydz \tag{6.7}$$

for $P_1 \neq P_2$.

Figure 6.2b schematically illustrates the mountain torque. The integration is in the same direction as the earth's rotation (West to East). If pressure is greater on the west side than on the east side of the mountain ($P_2 > P_1$), then atmospheric westerlies are slowed down which transfers

momentum to the Earth and thus Earth's rotation is sped up. Naturally, the far greater mass of the earth causes the change in motion of the atmosphere to be far greater than that of the solid Earth. More precisely, it is said that *easterly* momentum is added to the atmosphere when $P_2 > P_1$.

The final term in (6.4) is the friction integral. It is useful to obtain an expression for "F_x". To use molecular friction coefficients would be to greatly underestimate the magnitude of the actual frictional drag on the air. Instead, an analogy to molecular friction known as turbulent viscosity is used whereby the microscopic-scale molecular friction formulation is expressed in terms of macroscopic motions. The analogy proceeds by using a "mean free path" of a "blob" of air that is a similar concept to a mean free path of a molecule. The analogy is appropriate because the blobs have pressure forces acting on them that may be analogous to the collisions of molecules. One chooses an *eddy* coefficient of viscosity κ_E and assumes the processes involved are the same. For example, F_x might be defined

$$F_x = \kappa_E \nabla^2 \overline{u} \tag{6.8}$$

For *molecular* physics, the coefficient is a constant; here it is not. κ_E varies with the stability of the atmosphere, surface roughness, wind speed, etc. κ_E is very much bigger (a blob has billions of molecules) than the molecular coefficient, which refers to individual particles.

The friction integral is small in the free atmosphere, so the prime contribution is from the surface dissipation. Thus, the friction integral can be approximated in terms of stress tensors, τ

$$\int_V R_c F_x dV = -\int_V \left(\frac{\partial R_c \tau_{xx}}{\partial x} + \frac{\partial R_c \tau_{xy}}{\partial y} + \frac{\partial R_c \tau_{xz}}{\partial z} + \frac{\tau_{xy} \tan\phi}{r^2} + \frac{\tau_{xz}}{r^2} \right) dxdydz \tag{6.9}$$

The subscripts of the tensors denote components, not derivatives. In the x direction, for example

$$\kappa_E \nabla^2 \overline{u} = \nabla \cdot \tau$$

where $\boldsymbol{\tau} = (\tau_{xx}, \tau_{xy}, \tau_{xz})$ and the "∇" operator above is three-dimensional. The stress tensor can be thought of as stresses applied to the sides of a small cube. The first subscript denotes the direction of the motion that is affected (in this case x, because momentum M depends upon u). The second subscript denotes the direction of the axis normal to the given face of the cube. Hence, τ_{xx} is the pressure force in the x direction, whereas τ_{xz} is a stress caused by vertical shear of motion in the x direction. (See Figure 6.3). One expects the frictional interaction with the ground to exceed the internal atmospheric friction, so τ_{xz} will dominate in the surface boundary

layer. If the horizontal components of τ are ignored, then the vertical integral in (6.9) reduces to evaluating the stress tensor at the earth's surface.

$$\int_V R_c F_x dV \approx -\int_{x_0}\int_{y_0} R_c \tau_{x_0 z_0} dy_0 dx_0 \tag{6.10}$$

Stanton (1911) introduced the concept of a drag coefficient and Taylor (1916) suggested that stress be proportional to velocity squared. An approximate formula for the vertical stress tensor component may be defined as:

$$\tau_{x_0 y_0} = \mu \rho_0 u_0 \sqrt{u_0^2 + v_0^2} \tag{6.11}$$

where $\mu_M \sim 4 \times 10^{-3}$ and has no units. Using **Error! Reference source not found.** to approximate the friction force yields:

$$\int_V R_c F_x dV \approx \int_{x_0}\int_{y_0} R_c \mu \rho_0 u_0 \sqrt{u_0^2 + v_0^2} dy_0 dx_0 \tag{6.12}$$

where the subscript zero refers to values measured at standard anemometer height. The surface stress is always dissipating atmospheric motion, but the right-hand side of **Error! Reference source not found.** can be positive. Friction can increase M if the surface winds are easterly ($u_o < 0$). Since the main contributor to the friction torque is from stress applied at the Earth's surface, then the sign of this term should largely agree with the sign of the surface zonal wind. Hence, friction slowing down surface westerlies has negative value while slowing down easterlies is positive since friction is 'adding' westerly momentum to those easterlies.

A torque upon the zonal flow can be created when sub-grid scale gravity waves break and dissipate. Since the gravity wave breaking causes a drag, one might include it in a general concept of frictional dissipation. McFarlane (1987) reviews development of the concept and discusses formulation and calculation.

Huang and Weikmann (2008) discuss several ways to calculate the mountain torque from gridded data. But first, one can anticipate some broad properties of this torque from SLP maps. The sign of the mountain torque is negative for higher pressure on the west side and lower pressure on the east side of a North-South oriented mountain range. Negative sign opposes westerlies or reinforces easterlies. The mountain torque is generally negative in NHem and SHem middle latitudes. Because the Andes are the dominant mountain range in the SHem midlatitudes, one can easily anticipate the negative mountain torque there from Figure 4.4. The subtropical high off the west coast is coupled with lower pressure east of the Andes. Similarly, a

negative mountain torque can be created is via a persistent lee-side (East side) trough for westerly flow blowing over a North-South oriented mountain range, such as the Rockies. In the tropics, positive values of mountain torque occur which implies higher pressure to the East side and lower on the West side of topographic features. Positive tropical values of mountain torque are apparent in SLP values straddling the eastern African highlands (~15N in Figure 4.4a during DJF and ~15S in Figure 4.4c during JJA).

Water vapor is generally ignored in AAM tendency because the vapor is generally a small percentage of the total atmospheric mass. However, water vapor can be producing a torque due to the transport of water out of the subtropics towards higher and lower latitudes; Egger (2006) estimates this torque to have a magnitude of ~1 Hadley.

6.1.3 Estimated Tendency Values

Zonal and time mean: mountain, friction, and gravity wave drag torques are shown in Figure 6.4. The figure (redrawn from Huang, et al., 1999) also compares data from Newton (1972; shown in Grotjahn 1993) with a modern reanalysis. The seasonal friction and mountain torques may be compared with Figure 6.5a,b where those torques are discussed more fully. The annual mean frictional torque (Figure 6.4c) is largely as one expects from surface winds that are easterly between ~30 S and ~30 N with peak values near 15 S and 15 N. The midlatitude westerlies have large negative values. Annual average values are stronger in the SHem due to the greater ocean coverage (Figure 1.1) in the tropics and less seasonal change in the midlatitudes. (Ocean areas tend to have stronger surface wind speeds as implied by Figure 6.6.) Gravity wave drag torque appears smaller (or at least more localized) than the frictional torque (Gong et al., 2019) for the troposphere and lower stratosphere, but it is likely much more important in the mesosphere (Holton, 1982). In Figure 6.4d the gravity wave drag is largest between about 25 N to 50 N during DJF, negligible during JJA when the annual mean is similar to DJF but halved in magnitude.

The spherical coordinates form of the angular momentum tendency equation can be found in various sources. The equation in isobaric coordinates and for angular momentum per unit mass (i.e. the absolute angular velocity) can be found in Karoly et al. (1998) and is reproduced here:

$$\frac{\partial[\overline{M}]}{\partial t} = -\frac{1}{R_c}\frac{\partial}{\partial\varphi}\left\{\Omega R_c^2\cos\varphi[\overline{v}] + \underbrace{R_c\cos\varphi\left([\overline{u}][\overline{v}] + [\overline{u''v''}] + [\overline{u}'\overline{v}']\right)}_{(Ruv)}\right\} \quad (6.13)$$
$$-\frac{\partial}{\partial p}\left\{\Omega R_c^2\cos\varphi[\overline{\omega}] + R_c\cos\varphi\left([\overline{u}][\overline{\omega}] + [\overline{u''\omega''}] + [\overline{u}'\overline{\omega}']\right)\right\} + g\frac{\partial Z}{\partial\lambda} - R_c g\frac{\partial}{\partial p}[\overline{\tau_\lambda}]$$

The subscript λ on τ indicates the zonal component of the stress tensor. One notable difference from (6.3) is the additional *cosφ* factors in the horizontal and vertical flux terms. Because *cosφ* decreases towards each pole, the terms inside the meridional derivative (such as the group labelled '*Ruv*') decrease more rapidly towards the poles than in (6.3). The form (6.13) was used for Figure 6.5. However, the tendency term and the two pressure derivative terms in (6.13) were not directly calculated by Karoly et al. (1998). The pressure derivative term on the RHS vanishes by presenting vertical integrals of this equation. Unlike the previous figure, the friction term in Figure 6.5 is defined as a residual from calculating the remaining terms on the RHS and presumed to be mainly from torque due to surface stress. Vertical integrals of the remaining terms on the RHS of (6.13) are shown in Figure 6.5a,b. Note that the middle term in *Ruv* includes all transients, eddy and zonal mean; but Karoly et al. call this quantity by its primary contributor, transient eddies; that approximate labelling is adopted here.

The estimates of friction in Figures 6.4a,b and 6.5a,b have broad agreement. The patterns are similar to the annual average data of Figure 6.4c, with two obvious seasonal modifications: stronger values in the winter hemisphere middle latitude westerlies and the tropical peak values linked to the winter hemisphere Hadley cell. A closer look reveals notable differences. During DJF, the midlatitude friction peaks near 45 S in Figure 6.4a, while the JFM residual peaks near 50 S in Figure 6.5a. The DJF SHem tropical max has a single peak near 25 S whereas the JFM residual has peaks near 35 S and 25 S. During NHem winter, the peak positive is near 12 N and similar magnitude in both calculations. The NHem midlatitude extreme in friction is near 35N in both datasets and almost twice as strong in the residual calculation. With the exception of 15 S, the older data (Newton, 1972) agrees well with Huang et al. (1999). The SHem wintertime midlatitude values (Figures 6.4b and 6.5b) are very similar in location and magnitude in both figures; compared to summer, the friction reaches similar peak value but the peak is much broader and negative values spread over adjacent latitudes. The SHem winter Hadley cell peak near 15 S is about 20% larger in Huang et al. than in the residual calculation. Other relative

extrema are similar in both figures with some peak values slightly larger in the residual than in the direct estimates shown in Figures 6.5b and 6.4b, respectively. Though different years and datasets are used, the sign of the friction in Figure 6.4a,b match well the surface winds in Figure 4.13. Negative friction values from ~67 S to ~35 S and ~30 N to 60 N in Figure 6.4a match well surface westerlies Figure 4.13a during DJF. Similarly for JJA, negative friction from ~65 S to ~30 S and ~35 N to ~65 N are consistent with Figure 4.13b. Positive friction is found for most latitudes in between (except ~5 N to ~15 N during JJA) matching expectations from Figure 4.13.

The annual cycle of friction torque peaks (negative) during Austral late winter; but when combined with gravity wave drag (GWD) estimates, the combined torques are more comparable in Boreal and Austral winters (Egger et al., 2007; their Fig 5).

The mountain torque term in Figures 6.4a,b,c and 6.5a,b is generally: i) the same sign and ii) smaller amplitude than the friction term. This fact could be exploited to approximate the mountain torque in a calculation by boosting the friction – however, the amount of boost would vary with latitude and season, and the amount would approach doubling at a few places (e.g. 25N during DJF). Lorenz (1967) felt that this sign matching was fortuitous, and indeed there are regions where the signs differ (~15 N to ~20 N and ~35 N to ~40N during JAS; ~30 S to ~40 S during JFM). Though generally smaller in magnitude than the friction term, there are exceptions where the mountain torque is: a) comparable to the friction residual (~45N to ~55N, both seasons) and *larger* than the friction and largely opposing the horizontal transport: ~65N to 75N during JFM and ~10N to ~15N and ~30N to ~40N during JAS. Tropical values generally have larger peak mountain torques in the winter hemisphere with similar magnitude in both calculations. Middle latitude mountain torque values are generally larger in the NHem and slightly larger in the residual calculation. The older data shown (from Newton, 1972) generally agree well with more modern data. The mountain torque peaks in Boreal fall and Boreal spring (positive peak values) but the unresolved topography in the reanalysis data are assigned to GWD which is often large and negative (Egger, 2007). (Convection and other imbalances also contribute to the GWD term.)

The figures here show multi-decade time average values of the mountain torque. This torque has large swings (including sign) on shorter time scales (e.g. daily values). It seems generally true that friction operates on a longer time scale than the mountain torque. Egger et al. (2007) use lagged covariance to show peak *M* following about 3 days after a peak (positive)

mountain torque anomaly, while peak *M* follows 15-20 days after a peak (positive) friction anomaly; the autocorrelation decays much more slowly for friction than mountain torque as well. While friction has more power than the mountain torque at low frequencies, the relative importance flips for shorter time scales than about a month. For periods less than a fortnight, the orographic torque power spectrum is an order of magnitude (~10x) larger than friction (e.g. Iskenderian and Salstein, 1998). Huang and Weickmann (2008) show daily values (averaged over the whole Earth) that are more than 10 times as large as those shown in Figure 6.4c and those global averages range from large positive to large negative values.

The horizontal transport convergence is also shown in Figure 6.5a,b and it has generally larger amplitudes than the mountain torque. Peak horizontal transports are two to three times the largest magnitudes of the mountain torque. The horizontal convergence has peak magnitudes in the midlatitudes (especially during winter) and secondary peak values in the subtropics of the winter hemisphere. Given the mountain torque's similarity to friction, it generally has the opposite sign to the horizontal transport.

As discussed in Appendix A, the zonal and time average northward relative momentum flux labelled "*Ruv*" in (6.13) can be partitioned to isolate various phenomena. Karoly *et al*. partition *Ruv* into: i) zonal and time mean meridional motions (MMC), ii) transient motions of any kind, and iii) time mean zonal deviations (stationary eddies) of any kind. Vertical integrals of these three contributions to the meridional flux of relative momentum are shown in Figure 6.5c,d. It was shown in Chapter 4 that zonal and time varying phenomena dominate the midlatitude pressure pattern (e.g. Figure 4.3). Also shown previously is the winter hemisphere subtropics and tropics are dominated by the winter hemisphere Hadley cell (e.g. Figure 4.9). Accordingly, the fluxes shown in Figure 6.5c,d are consistent. The (time and zonal mean) Hadley cell (a MMC) contribution is poleward and largest in the winter hemisphere subtropics. The transients (which could include a contribution by time-varying MMCs as well as traveling frontal cyclones) dominate the horizontal flux in the subtropical and middle latitudes (with peak values near the latitude of the subtropical jets (e.g. Figure 4.13). The stationary eddies (which could include zonally-varying 'local' enhancements of the Hadley cells) are prominent only in the NHem (e.g. Figure 4.8). In NHem winter, the flux by stationary eddies is comparable in magnitude to the flux by transients, especially north of 45N. The eddies, both stationary and transient, can create a net meridional flux only if they have horizontally tilted troughs as will be

discussed more deeply in sections §6.2.1 and §6.2.2. The mean meridional cells create a net flux because often the meridional and zonal components *both* flip sign (e.g. Figure 4.9) from lower to upper troposphere; though additionally, the westerly flow aloft (e.g. Figure 4.13) often dictates the sign in the subtropics.

Returning to the momentum equation, because the flux has a peak near 30-45 degrees latitude in each hemisphere (depending on the season) the meridional derivative in (6.13) will flip sign near there (subject to the transcendental functions of latitude). Hence, *there is generally divergence of momentum out of the tropics and convergence in middle latitudes poleward of the peak flux and thereby poleward of the subtropical jet*. One might think that the convergence would be greatest at the jet, but no. This latitude offset is better understood later when looking at the kinetic energy equation.

To gain a sense of the horizontal variations in the axial AAM and two torques, Figure 6.6 is shown. The annual mean planetary part of axial AAM is large and symmetric about the equator it varies notably as $cos^2 \varphi$. The annual mean AAM (zonal) wind component depicted in Figure 6.6a has elements one can anticipate from figures in Chapter 4, especially larger positive values associated with the jet streams. Specifically, if one mentally combines the seasonal plots of Figure 4.13, the jet stream maxima lying at the east coast of NHem continents are thus extrema in Figure 6.6a. The relative maximum AAM north of New Zealand is primarily a winter (JJA) subtropical jet. The strong westerlies in the SHem midlatitudes are also as expected. The AAM maxima south of Africa is built more during summer (DJF) than winter. The tropical AAM having a negative zonal average is consistent with expectations from the seasonal plots of Figure 4.13. The stronger negative values of AAM over the tropical western Pacific seem more consistent with the stronger easterlies anticipated from the DJF stream function of Figure 4.17.

The horizontal variations of the friction torque (Figure 6.6b) can largely be anticipated from the four seasonal means of 950 hPa winds depicted in Figure 4.8. The circulation around the subtropical highs over the oceans has easterly "trade winds" on the equatorial side and westerlies on the poleward side; these flows are reflected in stronger friction torques in all five ocean basin subtropical highs. The oceanic westerlies of the SHem midlatitudes are both persistent and strong and lead to large negative annual mean friction torque. Where winds tend to have a clear onshore component the friction torque magnitude is stronger than elsewhere over land. For example, northeastern South America's large positive values are from easterlies visible

in Figure 4.8 that occur year-round. However, the negative values over India's west coast are mainly created during the Asian summer monsoon flow (JJA). Other areas of positive extremes occur where westerlies encounter north-south oriented mountain ranges (the Rockies and the southern Andes) and similarly for easterlies (southeast Africa).

The mountain torques (Figure 6.6c) show that zonal and time averages of the term are small differences between very large values to either side of the mountain range crest. These parallel bands arise from the local topographic slope. The $\partial p/\partial \lambda$ part of the mountain torque term flips sign from the west to east sides of north-south mountain ranges. As mentioned above, the mountain torque similarity (or not) to the friction torque changes when one considers different time scales. So, the depiction in Figure 6.4 hides a lot of complexity.

6.1.4 Additional Considerations

Atmospheric angular momentum interacts with the other major Earth systems, specifically the oceans and solid Earth. Oceanic angular momentum may be estimated from ocean currents (Peixoto and Oort, 1992). Winds apply stress to the ocean surface that generate currents of the wind-driven circulation (introduced in Chapter 1) and more generally change the elevation of the sea surface. Variations in the sea surface cause corresponding variations in the pressure applied to the solid Earth; analogous to the atmospheric mountain torque, change of sea surface elevation across an ocean basin creates a "continental torque". Currents at the ocean bottom apply a frictional stress to the seabed, thereby applying a frictional torque upon the solid Earth. This bottom friction torque appears to be much smaller than the continental torque.

The ocean surface responds such that sea level is in balance with the currents and the surface wind stress. The subtropical ocean gyres have peak elevations at latitudes that lie between the stronger atmospheric surface stresses of Figure 6.6b. These major subtropical ocean basin gyres tend to have highest sea level elevation towards the western side of the basin. However, the poleward flow is concentrated into a WBC so the sea surface changes rapidly with longitude such that the elevation difference between the eastern and western coastlines is considerably less than between the coast and the peak interior ocean elevation. Winds blowing onshore will drive up the coastal sea level as winds offshore drive down the coastal sea level. The ocean surface wind field may be visualized from Figure 4.8. Generally, the tropics have easterly motion which will raise the sea level on the western side compared to the eastern side of

each basin. In middle latitudes the zonal gradient of sea elevation is the opposite, with higher elevations on the east side. However, continental torques (estimated from general circulation modeling) are more often negative, implying dominance by the tropical slopes. Yoshioka et al. (2002) separate the gyre-producing winds from winds normal-to-shore to obtain rotational and non-rotational wind stress, respectively. They then use time-varying realistic surface winds, so separated, to drive a shallow-water system of equations and find that the non-rotational winds create most of the continental torque. Some results from this model are shown in Figure 6.7. The rotational-wind driven gyres dominate the sea level displacement (recall Figure 1.6). While the non-rotational wind displacements are much smaller in magnitude they do account for most of the difference between the eastern and western sides of the ocean. As anticipated, Figure 6.7b reveals the generally westerly flow of middle latitudes causes sea level displacement to be higher on the eastern side and lower on the western side of a middle latitude line. Similarly, the tropical easterlies create higher displacements on the western than on the eastern shores of the ocean basins. These properties are more easily seen in the Pacific and Atlantic oceans than in the Indian Ocean.

Angular momentum of the Earth (solid, gas, and liquid components) being conserved, means that changes in the amount of AAM can conceivably alter the rotation rate of the Earth and therefore change the length of the day (LOD). In thinking about the seasonal change of the zonal wind (Figure 4.13), it is clear that AAM should be less during boreal summer. Figure 4.13 shows the NHem having much greater seasonal change than the SHem so the NHem seasonal change is driving much of the *seasonal* AAM change. Sub-seasonal changes in LOD can be large and their timing more complex. The mass of the solid and liquid Earth is far, far greater than the atmospheric mass, so the seasonal LOD change is very small – a few milliseconds. Such small changes in LOD are measureable using very long baseline interferometry (correlating signals at widely separated radio telescopes of waves emitted from extremely distant quasars (Carter and Robertson, 1986). Various processes can change the LOD (e.g. Volland, 1996) however atmospheric processes generally dominate. Sharp readers might wonder about the transfer of AAM to the solid Earth by friction when most of the Earth's surface is covered by oceans. The transfer of momentum from ocean to solid Earth is rapid, within a few days (Ponte and Rosen, 2001). Consequently, daily values of the LOD and AAM are highly correlated (e.g. Carter and Robertson, 1986).

Juckes et al. (1994) compare and contrast the "transformed Eulerian mean" (TEM) and isentropic views of the zonal mean meridional circulations, including how the pressure gradient and geostrophic Coriolis terms can be canceled leaving an "ageostrophic" Coriolis term: $f v_a$ in the net. The TEM context has a version of the zonal momentum tendency equation with the momentum tendency related to divergence of the Eliassen-Palm flux. That EP flux links heat and momentum fluxes by introducing a "residual circulation". One might anticipate this linkage would be useful for understanding AAM tendency. However, in the context of the AAM tendency, Egger and Hoinka (2008) find the TEM formulation introduces much complexity without adding any new insight into angular momentum balance. In theta coordinates the Montgomery potential gradient in the momentum equation provides some forcing as a 'form drag'. However, Egger and Hoinka (2014) apply TEM to diagnose wave forcing of zonal mean AAM in θ (and other) coordinates.

Those readers interested in more depth on angular momentum are directed to reviews such as Egger et al. (2007). Here, more is presented about the momentum flux after consideration of how the westerlies are maintained against friction. That topic sets up discussion of jet streams and momentum tendency in the context of kinetic energy tendency.

6.2 Momentum Fluxes

Above, eddy momentum fluxes are shown to be a major factor in maintaining AAM. In this section, these fluxes are examined specifically, including: how they are created, where they are larger, and how they are linked to the MMC.

6.2.1 *Eddy structure to maintain zonal momentum against friction*

This subsection examines the question: how is zonal momentum maintained when opposed by friction? One might answer the question by a thermodynamic argument. Namely, the distribution of net radiation creates a pole to equator temperature gradient that in turn (from the hypsometric equation) creates a pole to equator geopotential gradient and (from geostrophic balance) creates westerlies. In short, the uneven distribution of radiation maintains the momentum. The traditional description of this process using energetics is via a conversion from (available) potential energy set up by the uneven radiation into kinetic energy. That process is

detailed in the next chapter. Here the focus is to gain a deeper appreciation of the transport term "Ruv" in the zonal momentum tendency equation (6.13).

As shown in Figure 6.5, the momentum transport peaks in midlatitudes and it is dominated by transients and stationary eddy momentum fluxes. The primary contributor to the momentum fluxes by transients are transient eddies, both frontal cyclones and time-varying longer waves. In a remarkable bit of intuition, Jeffreys (1926) found not just an explanation for the transport, but also uncovered a key property large atmospheric eddies must have in order to accomplish the transport. He first focused on the planetary boundary layer but ended up predicting structures in the upper air flow -- without the benefit of upper air observations! His predictions were not verified with certainty until two decades later.

Jeffreys began by showing that the zonal average flow cannot accomplish the transport. Consider how the zonal mean of geostrophic meridional wind is zero. He next showed that transport of momentum in a frictional boundary layer would not transport enough momentum. Finally, it followed that an *eddy* horizontal momentum flux was the major mechanism for maintaining the angular momentum balance. He needed a way to have a net zonal average covariance of $[uv]>0$ such as with northeasterlies mixed with southwesterlies. Eddies could transport the momentum poleward even if the winds are geostrophic, as long as those eddies have a particular *shape*. In short, he demonstrated that eddies are *fundamental* to the general circulation and he predicted their shape. His arguments are sketched below using observed magnitudes of observations.

A starting point is to estimate the frictional loss of momentum. The earth is nearly spherical and, to be strictly correct, curvature terms should be included. However, a Cartesian coordinate system is acceptable for illustrative purposes as the loss will be calculated for a column of unit horizontal area. Numbers similar to Jeffreys' are used first and some better estimates tested later. From the linear momentum equation, Jeffreys proceeded to determine what the rate of dissipation would be. He chose $u_0 = 4$ ms^{-1} for the horizontal average value of surface zonal velocity. Using Cartesian geometry, the frictional loss by an air column interacting with the surface of the earth may be approximated by

$$\int_{\text{vol}} F_x d\text{vol} = \int_{X_0}\int_{Y_0} \mu\rho_0 u_0 [u_0^2 + v_0^2]^{\frac{1}{2}} d\text{Area} \qquad (6.14)$$

Approximate values may be substituted into (6.14) to estimate the rate of extraction from a column of unit horizontal area. Assumed are: the meridional velocity of 1 m/s and $\mu = 4\text{x}10^{-3}$. These choices obtain:

$$F_{xr} = \int_{\text{vol}} F_x d\text{vol} \sim (4\times10^{-3})(1\,kg\,m^{-3})(4\,ms^{-1})(4.123\,ms^{-1})(1\,m^2) \simeq 6.6\times10^{-2}\,N \qquad (6.15)$$

as the rate of loss.

How large is this loss of momentum? One answer is to compare this rate to the amount of momentum in the atmosphere and from that information estimate how fast the atmosphere loses its momentum. The total amount of momentum in the column as estimated by Jeffreys is

$$M_L = \iiint \rho u\, dz\, d\text{Area} = \int_0^{P_0} \iint \frac{u}{g} d\text{Area}\, dP = P_0 \left(\widetilde{\frac{u}{g}} \right) \iint d\text{Area} \qquad (6.16)$$

$$= \frac{(4\,ms^{-1})(10^5\,Pa)(1\,m^2)}{9.8\,ms^{-2}} = 4x10^4\,N\,s$$

A very rough first estimate of the time (t_{xc}) to lose all the zonal momentum is found by assuming the rate of loss is constant and independent of wind speed, i.e. $t_{xc} = M_L / F_{xr} \approx 6x10^5 s \approx 7$ days. This simple calculation indicates a fast rate since all momentum would be lost in about a week. This estimate has several rather obvious flaws. Would correcting some major flaws make enough difference to change our perspective? Consider these two changes.

First, the linear momentum M_L is too small. The vertical average zonal winds in Figure 4.13 are much stronger than 4 ms^{-1}. The vertical mean of $[u]$ is ≥10 ms^{-1} in middle latitudes and ~20 ms^{-1} at the subtropical jet latitude during winter. These raise the estimate of M_L by factors of 2.5 to 5 and thus t_{xc} might be 2.5 to 5 weeks for a constant frictional loss within the PBL.

Second, friction is proportional to the wind speed as (6.14) shows. Hence, as the atmosphere slows down, the rate of frictional loss, F_L must decline. A crude, speed-dependent friction can be added by noting that the frictional loss in (6.15) is proportional to wind speed squared. Therefore, assuming spin down of the flow is governed by

$$u_t = -au^2 \qquad (6.17)$$

then a is a positive constant controlling the rate of damping. The solution of (6.17) is

$$u^* = u(t) = (b + at)^{-1} \qquad (6.18)$$

where b is a constant of integration such that $1/b$ defines the initial amplitude $u(0)$. The velocity u^* asymptotically approaches zero, so one must discuss the loss of momentum in terms of a fractional change in the velocity. For comparison purposes, the time over which 80% of the original momentum is lost is used. From (6.18), the time is $(0.8\ b)/(0.2\ a)$. Using values for b and a that correspond to the velocity in (6.16) and rate of decay in (6.15) at the initial time, then

$$b = u(0)^{-1} = 0.25\,\mathrm{s\ m^{-1}} \tag{6.19}$$

and

$$\begin{aligned} a &= (\mu = 4\times10^{-3}) \times (\text{scale height} \simeq 8.4\ \mathrm{km})^{-1} \\ &\simeq 5\times10^{-7}\,\mathrm{m^{-1}} \end{aligned} \tag{6.20}$$

The measure of the density-weighted depth of the atmospheric column used is the scale height. From (6.19) and (6.20), the time to lose 80% of the momentum is about 2×10^6 seconds or 23 days when the friction varies as au^2. In contrast, the constant rate given by (6.15) loses 80% of the initial momentum (6.28) in about 5.5 days. The precise time is not so important as to note that friction removes linear momentum at a pretty fast rate. Hence, friction cannot be neglected during a season or even over a single month.

How is the circulation maintained against this loss? To balance the frictional loss, (6.4) has mountain torques and meridional fluxes of zonal momentum through latitude boundaries. Mountain torques can be ruled out, because they generally have a sign reinforcing the loss of momentum by friction on a long time average. Also, seasonal mountain torques are smaller than friction as shown in §6.1.3. To answer this question consider Jeffreys' model again.

Geostrophic winds are assumed above a planetary boundary layer (PBL) so the meridional transport of momentum to replenish the frictional loss is only possible by ageostrophic motions in the PBL.

For simplicity, assuming the constant rate of decay means that something must be replenishing the momentum at a rate of M_L per week. The transport into the domain from the meridional wall flux term in the angular momentum tendency equation, e.g. (6.5), must balance this rate of loss. Mathematically,

$$R\int_t\int_z\int \rho uv\,dx\,dz\,dt \simeq \iiint \rho_0 R\mu u_0 (u_0^2 + v_0^2)^{\frac{1}{2}}\,dx\,dy\,dt \tag{6.21}$$

The flux through the meridional wall is on the left-hand side of (6.21). The flux in (6.5) has a second part: $f\left[\tilde{v}\right]$ and that part of the flux through the meridional wall is assumed to be

negligible over time scales of a year since such a net shift of mass would violate mass conservation. Positive sign in (6.21) indicates northward flux across the lower latitude wall. The transport across the higher latitude is set to zero when located at the pole. Alternatively, a higher latitude wall can be incorporated into the left-hand side of (6.21) too. Following the discussion in §6.1.3, the long time average mountain torque usually has the same sign as the friction, so mountain torque can be assumed to be incorporated into (and to increase) the friction term on the right-hand side of (6.21).

Above an Ekman boundary layer, a model having geostrophic winds precludes a zonal average meridional motion (away from the possible zonal pressure imbalances across mountains). Hence the only meridional transport of zonal momentum must occur in the boundary layer of such a model. Therefore, the vertical integral in (6.21) is zero outside that boundary layer. A steady state may be assumed, which eliminates the need for the time integrals. For simplicity, Jeffreys let the velocities be constant within and outside of the boundary layer. Equation (6.21) becomes

$$R\rho u_0 v_0 \int_z \int dx\, dz \simeq \rho_0 R \mu u_0 \left(u_0^2 + v_0^2\right)^{\frac{1}{2}} \iint dx\, dy \qquad (6.22)$$

As above, $u = u_0 \simeq 4$ ms^{-1} throughout the depth of the atmosphere, and $v = 0$ except in the boundary layer, where $v = u/4 = 1$ ms^{-1} is used. For an Ekman flow, the wind crosses isobars from higher pressure (subtropics) to lower pressure (midlatitude storm track). For a region extending from 30 N to the North Pole with a 1 km deep boundary layer, the numeric values are

$$r\rho_o \left[\widetilde{uv}\right] \int_0^{2\pi} \int_0^{10^3} r \cos^2(\varphi)\, dz\, d\lambda = r\rho_o\, \mu u_o \left[\overbrace{\left(u_o^{\,2} + v_o^{\,2}\right)^2}\right] \int_{\frac{\pi}{6}}^{\frac{\pi}{2}} \int_0^{2\pi} r^2 \cos^2(\varphi)\, d\lambda\, d\varphi$$

$$7.5x10^2\, m^2 s^{-1} = (1\, ms^{-1}) \cos^2(30)(1\, km) \underbrace{\simeq}_{?} (12\times10^{-3}\ ms^{-1})(0.5)(6.6\times10^3\, km) = 322.6x10^2\ m^2 s^{-1}$$

(6.23)

The common $R\rho u_0$ is factored out, the value 0.5 is the average cosine of latitude for the domain, and 6.6×10^3 is the distance from 30° to the pole. A question mark is inserted below the equality since the right-hand side of (6.23) is about 50 times greater than the left-hand side. So the frictional dissipation exceeds the boundary layer transport by roughly a 50 to 1 ratio! Using speed-dependent decay would lower the right side, and boosting M_L would increase both sides.

But such refinements in the numerical estimates do not remove the large imbalance. Clearly, another process is needed.

Figure 6.5 shows that friction is balanced in midlatitudes by the eddies, especially the transient eddies. How can these eddies generate enough momentum transport if their winds are nearly in geostrophic balance? From Appendix A, the flux across the latitude boundary wall has a contribution from $[u'v']$. For NHem eddies to have a net northward flux, the eddies must have mainly southwesterly and northeasterly winds, and to have those winds their troughs and ridges must be *horizontally tilted*. SHem eddies need southward momentum transport and therefore mainly southeasterly and northwesterly winds. Sufficient meridional transport can be achieved if the eddies have horizontally tilted troughs (and ridges), as illustrated in Figure 6.8.

First consider troughs that are not tilted horizontally, i.e. the trough is either circular or the trough axis is oriented exactly north-south. In either case, there is no net northward flux as the contribution from $[u'v']$ on the west side is canceled by the contribution on the east side of the trough. Figure 6.8a shows the cancellation from this east-west symmetry for a NHem example. Circular troughs and ridges in both hemispheres have the same cancellation.

Second, introducing horizontal tilts makes the flow around the trough asymmetric, as shown in Figure 6.8b for a NHem low. A net zonal average $[u'v']$ occurs because the quantity is much larger on the east side than the west side as drawn. Also note that a southwest-northeast tilt results in a net northward flux while a northwest-southeast tilt results in a southward eddy momentum flux. Figure 6.8b illustrates a net convergence of eddy momentum at the central latitudes. Hence, eddies so tilted would build momentum of the zonal mean flow at the central latitudes. Building momentum means a gain in kinetic energy. From energy conservation, something must be losing energy and that is discussed in depth in the next chapter. Briefly, kinetic energy is being extracted from the eddy to feed the zonal average flow. This conversion between zonal and eddy kinetic energy is labelled ‘barotropic’ conversion, which is discussed in Chapter 1 and in more detail in later chapters. One can easily imagine an initially circular eddy (Figure 6.8a) being distorted *with* the flow of a jet stream at the central latitude (Figure 6.8b); what may be surprising is that this distorted eddy feeds kinetic energy into that jet by building the mean flow at the central latitudes. The converse is also true: an eddy with tilts *opposing* a jet at the central latitudes will *extract* momentum from that jet. This is a way to visualize barotropic growth of the eddy.

Figures 6.8a,b are idealized schematics. Given that eddies must transport a lot of momentum, how do tilted eddies appear in observations? Figure 6.8c illustrates a typical geopotential height pattern in the middle and upper troposphere in the NHem. Southwest-northeast oriented ridges and troughs are commonly seen in the NHem subtropics and midlatitudes and are visible in Figures 4.2, 4.3a, and 4.17a. Between such a pair of tilted ridge and tilted trough, the zonal winds are less than the zonal average while the meridional wind is equatorward resulting in $[u'v']>0$. Over northern Africa the subtropical jet is accelerating while also oriented slightly east-northeast resulting in positive meridional and zonal eddy wind components and $[u'v']>0$. In between that flux is zero where either component vanishes. In the SHem, a northwest-southeast tilt accomplishes the poleward (southward) momentum flux and is visible, but harder to see in those figures due to the strong zonal average flow and generally weak standing waves. The tilted troughs in the subtropics are more easily seen in the stream function (Figure 4.17) than in the height field. Near the Earth's surface, subtropical highs (recall Figure 4.4) are also tilted on time averages; Figure 6.8d shows how asymmetry in a typical time mean NHem subtropical high also has a net poleward transport of zonal momentum.

Returning to the momentum maintenance scale analysis, these tilted eddies can be incorporated and bring (6.23) closer to balance. For a tilted trough like Figure 6.8b, one can reasonably let $u' = v' = u_0$ on the east side of the trough and $u' = v' = -u_0$ on the west side. If this is done just in the PBL, then the left side of (6.23) is four times as large while the right side is $\sqrt{2}$ times as large. It is reasonable to assume that the tilted troughs extend through the depth of the troposphere (~ 10 km). Density decreases (approximately) exponentially with elevation but one can express the depth in terms of a scale height (possibly subtracting the stratospheric contribution) which further raises the LHS by a factor of six to seven. The LHS is further elevated by noting from Figure 4.13 that mid- and upper-troposphere winds on average are much stronger than 4m/s; reasonable values raise the LHS another factor of five. At this point the two sides are similar enough for this discussion. The point of this crude calculation is that Jeffreys deduced that the atmosphere must have deep tilted waves in the subtropics and middle latitudes in order to maintain the general circulation *without upper air observations*!

Jeffreys' conclusion was finally confirmed by Starr (1948). Observations reported by Starr and White (1951) showed quite clearly that the angular momentum transport was primarily accomplished by the eddies. Theoretical models of linear instability on a sphere (e.g., Baines,

1976, or Fredericksen, 1978) also contain poleward momentum fluxes produced by the most rapidly growing solutions. The nonlinear extensions of these simplified theoretical models show this transport even better since the poleward transport is enhanced at high levels compared with linear models (e.g., Simmons and Hoskins, 1978).

6.2.2 *Contributors to zonal wind tendency*

The analysis in the last subsection emphasizes the role of eddies in maintaining the westerlies against frictional losses. The association is more complex than that. To understand this better, consider the zonal average zonal wind equation. Working with (C.25) and (C.23) in isobaric coordinates, the equation may be written as:

$$0=\frac{\partial[\bar{u}]}{\partial t}=\underbrace{-\frac{\partial}{r\partial\varphi}\left(\overline{[u''v'']}+[\bar{u}'\bar{v}']\right)}_{\text{"Eddies"}}-\frac{\partial}{\partial p}\left(\overline{[u''\omega'']}+[\bar{u}'\bar{\omega}']\right)$$
$$\underbrace{-[\bar{v}]\frac{\partial[\bar{u}]}{r\partial\varphi}}_{\text{"MMC"}}-[\bar{\omega}]\frac{\partial[\bar{u}]}{\partial p}+\underbrace{f[\bar{v}_a]}_{\text{"Coriolis"}}-F_x \qquad (6.24)$$

Here the pressure gradient term has been cancelled by the geostrophic part of the Coriolis term and the mountain torque is ignored.

Recalling Figure 6.5, the transients (mostly transient eddies) have largest values of momentum flux in the middle latitudes and are stronger in winter. The standing waves produce comparable momentum flux as well in the NHem winter subtropics and midlatitudes. So how are these transient and eddy fluxes distributed with longitude? To facilitate comparison with other figures, fluxes by all transients and by stationary waves are plotted in Figure 6.9. Also shown are the zonal averages for each field.

With a little additional knowledge about the frontal cyclone (eddy) life cycle, stationary waves, and the time mean winds, one can anticipate much of the zonal variation in this figure. Already shown (Figure 4.2) are the frontal cyclone storm tracks. Frontal cyclones are the primary contributor to the transient fields in middle latitudes. Shown in Figure 4.3, the eddy geopotential height magnitudes and RMS variance are largest on the downstream ends of the storm tracks. The stationary waves have zonal average fluxes in subtropical and middle latitudes mainly in the NHem during winter. The time average upper troposphere troughs in stream function (Figure

4.17) are prominent only in the NHem and generally near continental west coasts in the subtropics and the eastern continent in middle latitudes.

Figure 6.9 uses a representative level where the transient momentum fluxes tend to be largest: upper troposphere. The general patterns shown in the figure largely match those shown by Oort (1983; also reproduced in Grotjahn, 1993, Figure 5.16). The connection between zonal wind acceleration is best linked to the ageostrophic wind. This linkage is visible in the time average of the zonal wind tendency equation. Inserting (C20) and (C23) into (C26) yields

$$\frac{\partial u}{\partial t}+\frac{u}{r\cos(\varphi)}\frac{\partial u}{\partial \lambda}=-\frac{v}{r}\frac{\partial u}{\partial \varphi}-\omega\frac{\partial u}{\partial p}-\frac{1}{r\cos(\varphi)}\frac{\partial \Phi}{\partial \lambda}$$
$$+2\Omega\left(v\sin(\varphi)+\frac{\omega\cos(\varphi)}{\rho g}\right)+\frac{u}{r\cos(\varphi)}\left(v\sin(\varphi)+\frac{\omega\cos(\varphi)}{\rho g}\right) \qquad (6.25)$$

Writing (6.25) in flux form and applying the time average obtains:

$$\underbrace{\frac{1}{r\cos(\varphi)}\frac{\partial\overline{(uu)}}{\partial \lambda}}_{A}=-\frac{1}{r}\frac{\overline{\partial(vu)}}{\partial \varphi}-\frac{\overline{\partial(\omega u)}}{\partial p}+\underbrace{2\Omega\overline{v_a}\sin(\varphi)}_{C}+2\Omega\frac{\overline{\omega}\cos(\varphi)}{\rho g}$$
$$+\overline{\frac{u}{r\cos(\varphi)}\left(v\sin(\varphi)+\frac{\omega\cos(\varphi)}{\rho g}\right)} \qquad (6.26)$$

where the Coriolis and pressure gradient terms have been combined leaving the time average of the meridional component of ageostrophic wind: $\overline{v_a}$ in the Coriolis term ("C" in (6.26). Namias and Clapp (1949) concluded that the acceleration term "A" is approximately balanced by that ageostrophic Coriolis term in reference to accelerations and decelerations of the subtropical jet streams. (Ageostrophic winds are shown in Grotjahn.1993; Figure 5.7.) Poleward ageostrophic wind is consistent with westerly acceleration while equatorward motion is consistent with westerly deceleration. One notes that i) slowing down easterlies implies westerly acceleration and ii) the balance between terms A and C breaks down near the equator where C becomes small. The general pattern of the meridional component of divergent wind is similar to the corresponding ageostrophic wind component and the agreement is sufficient for the general discussion here. With that assumption, the divergent winds shown earlier (Figures 4.15 and 4.17) can enrich the interpretation of Figure 6.9

In the NHem during DJF, the larger transient fluxes (Figure 6.9b) are positive as anticipated from zonal mean data in Figure 6.5c. These larger values extend from the subtropical central oceans northeastward onto the continents in two groupings. The western grouping has peaks in the Pacific and in northern Mexico while the eastern grouping has an elongated peak over the eastern Atlantic across the northern Sahara. The two maxima in the western grouping and one elongated maxima near and over Africa are structures also found by Oort (1983). While the magnitudes in Figure 6.9 are similar to Oort's data over the continents, here the magnitudes are much larger over the oceans. The patterns and magnitudes here are more similar to the same quantity plotted in Karoly et al. (1998) using a different time period. Weak *negative* transient fluxes occur at the downstream ends of the Pacific and Atlantic storm tracks. At the end of those storm tracks the stream function of transient eddies tends to have a trough tilted generally northwest to southeast, resulting in the southward momentum fluxes. The lack of strongly negative values along a latitude circle is one reason why the transients have a large contribution to the zonal mean shown before.

Positive transient fluxes are either *poleward or upstream* of areas where: the subtropical jet streams are strongly accelerating in Figure 6.9a. The divergent wind generally has a poleward component (Figure 4.15a) near those accelerations. Further along the jet axis, the divergent winds tend to be from opposing directions along the downstream axis as one might expect from a jet axis at the hypothetical boundary between a "local Hadley" cell and a "local Ferrel" cell (called here an HCFC boundary). Zonal winds are accelerating near that subtropical Pacific maximum (though it is a little hard to see since the eastward extension of the Asian subtropical jet to the north has stronger (but decelerating) winds at those longitudes (180-140W). Since the transient fluxes are largest poleward of the subtropical jet core (even as that jet core moves further north downstream) this means those transient momentum fluxes have a positive meridional derivative along the jet. From the zonal wind tendency equation, (6.24) such *divergence of transient fluxes acts to decelerate the time mean zonal wind precisely where the subtropical jet stream is accelerating.* Clearly some other term (or terms) exceeds the transient flux divergence to produce the acceleration of the subtropical jet seen in Figure 6.9a. The main term to produce the acceleration is the ageostrophic part of the Coriolis term. *Hence, the acceleration/deceleration of the subtropical jet can be linked to the mean meridional cells. Poleward of the peak transient fluxes there is momentum convergence in the meridional*

direction which is accelerating the midlatitude westerly wind broadly as anticipated from the analysis by Jeffries in the previous subsection and as expected by zonal mean momentum contributions as shown in Figure 6.5c. The eddy convergence also helps energize eddy-driven jets.

Moving to the stationary waves fluxes in the NHem during DJF (Figure 6.9c) these may be anticipated from the southwest-northeast tilted troughs and ridges in Figure 4.17a as was discussed in the last subsection. The larger positive fluxes near the North American west coast and the tropical Atlantic into the western Mediterranean are both represented schematically by the *left* side of Figure 6.8c. Inspecting time mean winds like Figure 6.9a, one anticipates $u'<0$ where $v'<0$ in both regions. The larger fluxes over the Sahara and near Japan are both approximated by the *right* side of Figure 6.8c. Inspecting time mean fields, one anticipates large $u'>0$ due to the low latitude of the subtropical jet there and stream function contours in Figure 4.17a signify $v'>0$. The stationary waves have larger peak values than the transients, also directed northward, but the zonal distribution is more complex than found for the transients. Hence their zonal means (right-side panels in Figures 6.9b,c) have similar NHem peaks. From roughly 60W to 60E, there are a pair of positive and negative diagonal regions between 10N and 45N. This pair of elongated regions creates convergence of momentum over the northern Sahara that is well aligned with the acceleration of the subtropical jet. Similarly, the largest flux values, over eastern Asia are south of the subtropical jet so the meridional derivative of the stationary wave fluxes is also negative where the Asian subtropical jet accelerates to its peak values. This acceleration over Asia is reinforced by divergent winds at 200 hPa that have a poleward component (Figure 4.15a). Downstream, the peak fluxes generally overlie the peak subtropical jet winds. Over Siberia and adjacent waters are southward fluxes creating a strong flux convergence just north of the subtropical jet. To the south of the East Asian subtropical jet and west of the dateline, a negative area of momentum flux creates flux divergence thereby reinforcing the deceleration of the Asian subtropical jet as it leaves the Asian continent. West of Europe, the gradients of the transient and stationary wave fluxes are in opposition from 30N-45N, but reinforce in the subtropics. In short, parts of the stationary wave flux distribution overcomes the transients in maintaining the subtropical jet.

An intriguing negative area, with a northwest to southeast orientation straddles the equator east of the dateline; on the west side of this area the meridional derivative of this flux is

negative and one also finds westerly winds crossing the equator exceeding 25 m/s in these data. Such westerlies can act as a waveguide for eddies to move between the NHem and SHem.

In the SHem during DJF, the subtropical jet is poleward of the peak (negative) values of momentum fluxes by transients across the south Atlantic and Indian Oceans. Thus the meridional derivative of the transient flux is also negative and consistent with zonal wind acceleration. The stationary waves contribution is small over most of the SHem except along a line that parallels the SPCZ, but on the East side of the SPCZ trough visible in Figure 4.17a. This line cuts across the equatorial and subtropical eastern Pacific.

During JJA, the transient fluxes are strong in the SHem but generally weak in the NHem (the exception being the peak value near Japan is comparable to DJF). The peak SHem transient fluxes lie to the north of the jet across the south Atlantic, a configuration with flux convergence where the subtropical jet is accelerating. However, in the south Atlantic the 200 hPa divergent winds are equatorward and thus opposing the flux convergence by the transients. The transient flux magnitudes peak along 30S, favoring the east side of each ocean basin. The peak values from the Indian Ocean across Australia into the western South Pacific are nearly co-located with the subtropical jet stream axis, so there is little eddy flux convergence to accelerate that jet. However, the 200 hPa divergent winds are poleward and thus can accelerate that jet as anticipated from (6.26). The transient eddy transport near the southern tips of Africa and South America are larger during summer in Oort (1983). In Figure 6.9 the SHem transient fluxes have comparable peak magnitudes in DJF and JJA but, more in line with intuition, they are clearly greater during JJA. Also during SHem winter, peak fluxes are consistently ~10 degrees further north. During JJA, the stationary wave fluxes are generally weak except for the eastern Mediterranean Sea and the tropical south Indian Ocean; the divergent winds in both locations are poleward at 200 hPa (Figure 4.15b).

In addition to some stationary waves fluxes, the Coriolis term in (6.24) is also generally working against the transient eddies. As is apparent from the similar quantity, divergent wind in Figure 4.15, the zonal wind acceleration is in a region with strong poleward divergent winds. Poleward divergent winds are consistent with a locally stronger ‘Hadley’ circulation. In the NHem and much of the SHem, where the meridional derivative of the transient flux is large and negative, implying momentum convergence and westerly acceleration, the divergent winds have an equatorward component that would decelerate the westerlies through the Coriolis term in

(6.24). This divergent flow is consistent with a locally stronger 'Ferrel' circulation. A SHem exception is between ~120E to ~140W in midlatitudes where divergent winds are poleward at 200hPa (Figure 4.15a). *This general, opposition between MMC circulation and the eddy flux convergences is no accident but arises from thermal wind shear balance*; the connection is explored further in the next subsection and more fully with the Kuo-Eliassen equation.

Having discussed the horizontal structures of the fluxes at a representative level, the vertical structures in the zonal and time average zonal wind tendency equation (6.24) are now considered. Technically, since a time average is applied, the time tendency term should be zero. Even though the long term daily mean [u] may change over a season, there is little trend over the course of extreme seasons defined by months DJF (or perhaps JFM) and JJA (or perhaps JAS) So, the terms on the RHS are expected to cancel when added together. The larger contributions arise from the three terms labeled in (6.24) and plotted in Figure 6.10. To assist with the interpretation, the MMC, subtropical jet, and easterly winds are shown schematically.

The first term on the RHS is labelled "Eddies" and shown in Figures 6.10b,f. The term consists of two parts. The first part is the meridional convergence of the meridional flux of zonal velocity due to all transients. The second part is the meridional convergence of the meridional flux of zonal velocity from stationary waves. It is a reasonable approximation to ascribe the bulk of the flux convergence of transient winds to transient eddies and those to midlatitude traveling frontal cyclones. The other two labeled terms come from the meridional flux of zonal average absolute vorticity by the zonal average meridional wind. That meridional flux is split into the relative vorticity flux (Figures 6.10c,g, the "MMC" term) and the planetary part (Figures 6.10d,h, the "Coriolis" term).

The "Eddies" flux convergence term during JFM, Figure 6.10b may be compared with information plotted in Figures 6.9b,c. The 200 hPa level in Figure 6.10b may be deduced from minus the meridional derivatives of the zonal averages shown in Figures 6.9b,c (ignoring differences in the years and months used, of course). In those prior figures the largest values of transients and stationary waves together are found in the NHem. On that basis one might expect the "Eddies" zonal mean flux divergence to be largest in the NHem. However, the transient flux in the SHem is not only not small during JFM, it has less variation with longitude than the corresponding NHem flux. From Figure 6.5c one anticipates the peak fluxes on the zonal mean to be negative near 40S and positive near 30N. *In midlatitudes*: taking minus the meridional

derivative to obtain a horizontal flux convergence in a zonal mean finds a positive maximum to the south of 40S and north of 30N along with corresponding a negative values north of 40S and south of 30N. Figure 6.10b shows this pattern with peak values near the 200 hPa level shown in the prior figure. In higher latitudes of the prior figures, one anticipates negative values from the stationary waves north of 60N and south of ~65S. Hence, these "Eddies" fluxes are building zonal mean westerlies in middle latitudes and extracting it in the subtropics and high latitudes. The larger divergences occur primarily in the middle to upper troposphere. The level of relative peak magnitudes declines towards the pole somewhat mirroring the declining level of the tropopause with increasing latitude (as deduced from Figures 3.20 and 4.9) Within a hemisphere, larger values are found during winter. During JAS the NHem contributions by both transients and stationary waves are greatly reduced; some positive values remain but the pattern is shifted northward and the peak values are 10-15 degrees poleward. A similar seasonal shift of the positive peak divergence occurs for the SHem. Compared with JFM, during JAS the SHem transients in Figures 6.9e,f zonal averages are: larger, but the midlatitude peak value shifted from 40S to 30S while the higher latitude extremum shifted little. Hence the gradient between those extremes has decreased for JAS. In turn, positive values in Figure 6.10f occur from 30S to ~65S with peak values slightly less than during JFM. The shift of the peak flux from 40S to 30S elevates the negative values of the flux convergence in the subtropics (15S to 25S). In short, the Eddies term has a "tri-pole" pattern in each hemisphere: a midlatitude positive region of momentum convergence that is broader during local winter and bracketed by two negative regions (momentum divergence). As for other variables, the seasonal change is less in the SHem.

The MMC term in (6.24) is plotted in panels c and g of Figure 6.10. Corresponding panels a and e help with the interpretation. The meridional shear part of the term will be larger in the upper troposphere and lower stratosphere because [u] is larger there (e.g. Figure 4.13). The meridional wind can be anticipated from flow in the meridional plane around the MMCs. As mentioned before (e.g. Figure 4.9 as well as in the top two panels, the winter hemisphere "Hadley" cell is much stronger than the corresponding summer cell. Hence the term is large (and negative) in the winter hemisphere tropics where meridional circulation is poleward. It is clear that on these zonal averages, the MMC term is reinforcing the "Eddies" term in the tropical winter hemisphere upper troposphere.

The remaining panels (Figures 6.10d,h) show the contribution from the Coriolis term defined using the ageostrophic meridional wind that in turn can be approximated from the MMC circulations on the top panels as well as plots of the MMCs shown before. The pattern follows the meridional wind portion of the MMCs. The meridional wind flows opposite directions in lower and upper troposphere and is stronger where associated with the Hadley cells. Multiply that flow by the Coriolis parameter. Since the Coriolis parameter a) flips sign between hemispheres with a hard zero at the equator and b) increases in magnitude towards the poles this term also flips sign vertically in the tropics. Evidence for "Ferrel cells" and even hints of "Polar cells" are also visible in this term. The plotted terms in Figure 6.10 are expected to largely cancel when added together if zonal wind change is very small. Therefore, the Coriolis term also has a "tri-pole" pattern in each hemisphere. Similar to the other terms, the upper maxima have highest elevation in the tropics and dip to lower elevations in polar regions. The Coriolis term adds westerly acceleration at upper levels in the tropics, where the Eddies term extracts westerly motion. The Coriolis term is larger and positive in the winter hemisphere where the MMC term substantially extracts westerly motion. At low levels, where the "Hadley" cells have generally equatorward flow, this term introduces easterly acceleration. (The easterly acceleration is not balanced by other terms shown in Figure 6.10 but one imagines the friction term, slowing down easterly winds in the PBL, largely provides the needed balance.) Given the Coriolis term's dependence upon $\left[\overline{v_a}\right]$, these accelerations of $\left[\overline{u}\right]$ in the tropics at lower and upper levels are consistent in sign with angular momentum conservation of air moving meridionally, as in the simple calculations shown in Figure 4.18. The Asian summer monsoon can be envisioned as part of an expansion of an Indian Ocean "local" Hadley cell leading to the northward flow north of the equator and contributing much to the near surface positive values in there during JAS (Figure 6.10h). Considering the middle latitudes, one sees again the opposition between the "Ferrel" cell motion wanting to decelerate the westerlies opposing the acceleration by the convergence of eddy momentum. This linkage between MMCs and eddy fluxes can be turned around to form an expression that deduces an MMC from convergence of eddy momentum flux in the next subsection.

6.2.3 *Eddy momentum fluxes linked to meridional cells*

As determined above, the transient eddy momentum fluxes in middle latitudes are opposed by the angular momentum changes produced by meridional motions within MMCs. This connection can be rearranged mathematically as eddy fluxes creating MMC motion.

Beginning with (6.2) and expanding the advection terms using the continuity equation

$$\rho \frac{dM}{dt} + \frac{R_c}{\cos\varphi}\frac{\partial P}{\partial \lambda} = -R_c F_x \tag{6.27}$$

Writing the meridional and vertical advection terms in (6.27) in flux form yields:

$$\frac{\cos\varphi}{\cos\varphi}\frac{v}{r}\frac{\partial M}{\partial \varphi} = \frac{1}{R_c}\frac{\partial\left(Mv\cos\varphi\right)}{\partial\varphi} - \frac{M}{R_c}\frac{\partial v\cos\varphi}{\partial\varphi}$$

and (6.28)

$$\omega\frac{\partial M}{\partial p} = \frac{\partial(M\omega)}{\partial p} - \frac{M}{R_c^2}\frac{\partial(\omega R_c^2)}{\partial p}$$

Substituting (6.28) into (6.27) and invoking the continuity equation (C.30) removes the divergence operator multiplying *M.* Taking a time average removes the local change term in (6.27) while taking a zonal average removes the longitudinal advection term. For simplicity, the mountain torque, arising from the zonal mean pressure gradient term, is dropped. The result is:

$$\frac{1}{R_c}\frac{\partial\left[Mv\cos\varphi\right]}{\partial\varphi} + \frac{\partial\left[M\omega\right]}{\partial p} = -R_c F_x \tag{6.29}$$

Expanding the quadratic terms into zonal mean and eddy parts, e.g. $[Mv]=[M][v]+[M'v']$ and applying the Chain Rule obtains:

$$\frac{[v]\cos\varphi}{R_c}\frac{\partial M}{\partial\varphi} + \frac{[M]}{R_c}\frac{\partial[v]\cos\varphi}{\partial\varphi} + [M]\frac{\partial[\omega]}{\partial p} + [\omega]\frac{\partial[M]}{\partial p} + \frac{1}{R_c}\frac{[u'v']rR_c}{\partial\varphi} + \frac{\partial[u'\omega']R_c}{\partial p} = -R_c[F_x] \tag{6.30}$$

Using the continuity equation again and moving the eddy flux terms to the RHS obtains:

$$\frac{[v]}{r}\frac{\partial M}{\partial\varphi} + [\omega]\frac{\partial[M]}{\partial p} = -R_c\left\{\frac{1}{R_c^2}\frac{[u'v']\cos^2\varphi}{\partial\varphi} - \frac{\partial[u'\omega']}{\partial p}\right\} - R_c[F_x] \tag{6.31}$$

Equation (6.31) can be interpreted as an equation for the MMC circulation $[v]$ and $[\omega]$ has the while the RHS has the eddy forcing terms. Defining the MMC strictly as zonal average flow in the meridional plane, one could expressing $[v]$ and $[\omega]$ in terms of a stream function, Ψ. One would specify M and the eddy fluxes from observations and solve (6.31) as a linear, second-order p.d.e. in Ψ.

As an equation for a MMC circulation is (6.31) too simple? Perhaps the mountain torque term matters? From Figures 6.4 and 6.5, this torque is much smaller than the momentum fluxes and it would be zero above the Earth's surface (locally). Something major contributes to the MMC that is missing from (6.31). To find it, recall that the derivation began with the zonal momentum equation. The Coriolis term mixes meridional and zonal winds. So, if one examines the corresponding meridional wind tendency equation, the pressure gradient term cannot be dropped, $\left[\partial p / \partial \varphi\right] \neq 0$. A meridional gradient of pressure develops from *meridionally-varying diabatic* processes (e.g. absorbed solar radiation that varies with latitude) as well as energy conversions (discussed in the next Chapter). Therefore, a fuller picture of the creation of MMCs also requires consideration of a thermal equation and the Kuo-Eliassen equation (in a later chapter) does just that.

6.3 Other Expressions of Zonal Mean Momentum

6.3.1. Net eddy forcing of zonal momentum: Eliassen-Palm fluxes

The prior subsection deduces MMC motion from eddy momentum fluxes but ends by noting that eddy heat fluxes are missing and will also play a role. While a full elaboration is left for Chapter 8, one can reveal a role for meridional eddy heat fluxes in a zonal mean meridional circulation while investigating the maintenance of zonal momentum using a popular diagnostic. That popular diagnostic is commonly referred to as the "E-P flux" vector, represented here by: $\mathfrak{F}$. The mathematics is developed below using a simplified form of a balanced set of equations.

The quasi-geostrophic (QG) system is sufficient to illustrate broadly the dynamics. Similar dynamical analogs have been derived for less restrictive equations (e.g. Andrews and McIntyre, 1976, 1978a, 1978b). Appendix C includes the QG system. The QG system can be derived using perturbation theory, where the Rossby number (*Ro*) is one of several nondimensional parameters using a small *Ro* expansion (e.g. Grotjahn, 1979). The lowest, or "zero" order system is in geostrophic and hydrostatic balance which, along with the ideal gas law may be combined to formulate a thermal wind shear relation as illustrated by (C.39). The next order, order "one" is QG balance where: all advecting and advected velocities are geostrophic winds. Vertical advection only appears in the potential temperature tendency (C.43) and

continuity (C.29) equations of the QG system. In the QG θ tendency equation the horizontal average static stability is large enough, even for small vertical motions, to cause the vertical advection to be potentially comparable to the largest terms in that equation. Hence the horizontal average θ on isobaric surfaces: θ_s is only a function of pressure.

To further simplify the mathematics, Cartesian geometry (C.19) and isobaric coordinates (C.23) are chosen. The continuity equation in this context is invoked to write the advection terms in "flux" form. Finally, zonal averaging is applied and any mountain torque created is neglected. Zonal averaging eliminates the zonal advection and zonal pressure gradient terms as they are perfect differentials on a periodic domain. (Hence mountain torques are ignored.)

The results of these simplifications for (C.41), (C.39), (C.29), and (C.43) are respectively:

$$\frac{\partial [u]}{\partial t} + \frac{\partial}{\partial y}\left[v_g' u_g'\right] = f\left[v_{ag}\right] + F_x = f[v] + F_x \tag{6.32}$$

Since $[v_g] = 0$.

$$\frac{\partial u_g}{\partial p} = \frac{R}{pf}\left(\frac{p}{p_{00}}\right)^{\frac{R}{C_p}} \frac{\partial \theta}{\partial y} \equiv G(p)\frac{\partial \theta}{\partial y} \tag{6.33}$$

Where (6.33) defines a local temporary function of pressure, G, used here to reduce clutter in this derivation.

$$\frac{\partial [v]}{\partial y} + \frac{\partial [\omega]}{\partial p} = 0 \tag{6.34}$$

$$\frac{\partial [\theta]}{\partial t} + \frac{\partial}{\partial y}\left[v_g' \theta'\right] + [\omega]\frac{\partial \theta_s}{\partial p} = D_T \tag{6.35}$$

Where D_T is the diabatic heating rate per unit mass.

Observationally (e.g. Holton, 2004) the divergence of horizontal eddy heat flux is largely cancelled by adiabatic heating or cooling by vertical motions of the statically stable atmosphere. By removing the portion that cancels, the remaining vertical motion can be ascribed to the presence of diabatic heating. Consequently, it is reasonable to combine the two terms on the LHS in (6.35) to define a vertical motion, $[\omega^\sharp]$ that is often labelled part of a "residual

circulation" in the meridional plane. It is "residual" in the sense of after accounting for adiabatic heating or cooling. Specifically:

$$\frac{\partial[\theta]}{\partial t}+[\omega]\frac{\partial\theta_s}{\partial p}+\frac{\partial}{\partial y}\left[v_g'\theta'\right]=[\omega]\frac{\partial\theta_s}{\partial p}+\frac{\partial}{\partial y}\left[v_g'\theta'\right]\frac{\frac{\partial\theta_s}{\partial p}}{\frac{\partial\theta_s}{\partial p}}=\left[\omega^{\#}\right]\frac{\partial\theta_s}{\partial p}=D_T \tag{6.36}$$

Hence,

$$\left[\omega^{\#}\right]=[\omega]+\frac{\partial}{\partial y}[v'\theta']\left(\frac{\partial\theta_s}{\partial p}\right)^{-1} \tag{6.37}$$

The geostrophic subscript has been dropped from *v'* to reduce clutter. Inserting (6.37) into (6.34) obtains an expression for a corresponding $[v^{\#}]$ that must also satisfy continuity:

$$\begin{aligned}&\frac{\partial[v]}{\partial y}+\frac{\partial\left[\omega^{\#}\right]}{\partial p}-\frac{\partial}{\partial p}\left(\frac{\partial}{\partial y}\left([v'\theta']\left(\frac{\partial\theta_s}{\partial p}\right)^{-1}\right)\right)=0\\&\frac{\partial[v]}{\partial y}-\frac{\partial}{\partial y}\left(\frac{\partial}{\partial p}\left([v'\theta']\left(\frac{\partial\theta_s}{\partial p}\right)^{-1}\right)\right)+\frac{\partial\left[\omega^{\#}\right]}{\partial p}=0\end{aligned} \tag{6.38}$$

leading to

$$\frac{\partial\left[v^{\#}\right]}{\partial y}+\frac{\partial\left[\omega^{\#}\right]}{\partial p}=0 \tag{6.39}$$

if

$$\left[v^{\#}\right]=[v]-\frac{\partial}{\partial p}[v'\theta']\left(\frac{\partial\theta_s}{\partial p}\right)^{-1} \tag{6.40}$$

Substituting this expression for $[v]$ in (6.32) obtains:

$$\frac{\partial[u]}{\partial t}+\frac{\partial}{\partial y}[v'u']=f\left[v^{\#}\right]+f\frac{\partial}{\partial p}[v'\theta']\left(\frac{\partial\theta_s}{\partial p}\right)^{-1}+F_x \tag{6.41}$$

Rearranging and combining terms

$$\frac{\partial[u]}{\partial t}+f\left[v^{\#}\right]=-\frac{\partial}{\partial y}[v'u']+f\frac{\partial}{\partial p}[v'\theta']\left(\frac{\partial\theta_s}{\partial p}\right)^{-1}+F_x\equiv\nabla_M\bullet\boldsymbol{\mathcal{F}}-F_x \tag{6.42}$$

Where the divergence operator $\nabla_M\bullet\boldsymbol{\mathcal{F}}$ is in the two-dimensional (y,p) plane. Eq. (6.42) defines the diagnostic, vector quantity $\boldsymbol{\mathcal{F}}$ here labelled the "QG E-P flux". The name arising from a related argument developed in a study of mountain waves by Eliassen and Palm (1961). Hence:

$$\mathcal{F} \equiv \left(-\left[v'u'\right] , f\left[v'\theta'\right]\left(\frac{\partial \theta_s}{\partial p}\right)^{-1} \right) \tag{6.43}$$

It is a subtle but important point to note that if $[\omega^*]$ is viewed as a "residual" then so is $[v^\#]$. Given that view, then (6.42) can be viewed as having three physical ways to alter the zonal mean flow. The first is due to meridional transport of planetary angular momentum (per unit mass) by the residual circulation. The second is by eddy forcing expressed by the $\nabla_M \bullet \mathcal{F}$ term. Thirdly, by friction (F_x) in the direction of the flow. This subtle point leads to statement such as: "$\nabla_M \bullet \mathcal{F}$ represents the sole internal forcing of the [zonal] mean state" by eddies (Edmon et al., 1980). Additional dynamical concepts follow.

6.3.2 *Eliassen-Palm flux dynamics*

For adiabatic flows that are stationary, every term in (6.42) is zero, including $\nabla_M \bullet \mathcal{F}$. The latter result, that $\nabla_M \bullet \mathcal{F}$ =0, is often called the "Eliassen-Palm theorem". For this situation, the eddy forcing by momentum flux divergence and heat flux divergence must exactly cancel. This situation also implies no time tendency in (6.36) and that $[\omega^\#]$ and $[v^\#]$ are also zero, an expression of the Charney and Drazin (1961) "non-acceleration theorem". This non-acceleration condition can be generalized to hold even for finite amplitude waves, as long as the QG equations still apply. Edmon et al., (1980) show this property using the QG potential vorticity equation whose meridional flux of potential vorticity ($v'Q'_{QG}$) equals $\nabla_M \bullet \mathcal{F}$ which equals zero.

The analysis so far has been for the quasi-geostrophic framework with pressure as the vertical coordinate. A problem with this framework is momentum transfer between the atmosphere and the surface is not handled correctly. To resolve that problem and to extend the analysis both beyond QG and to finite amplitude waves, various authors have recast the analysis in isentropic coordinates (e.g. Andrews, 1983; Tung, 1986; Tanaka et al., 2004). A notable difference in the potential temperature coordinates is a term in the vertical component of the Eliassen-Palm flux introduced by pressure variation zonally over potential temperature surfaces. In fluid dynamics, a "form drag" is introduced by a force acting normally to a surface (which distinguishes form drag from skin drag which is directed tangentially). Pressure is the weight of

the air above a point so it acts in the vertical dimension and by that reasoning this pressure variation term on isentropic surfaces is often called a “form drag”. This form drag term is an expression of the eddy heat flux found in the vertical component of $\mathfrak{F}$ in isentropic coordinates. (The isentropic vertical component of $\mathfrak{F}$ also includes diabatic and momentum flux terms on the slope of the θ surfaces (e.g. Tanaka et al., 2004). Analyses for “dry” potential temperature coordinates have been extended to “moist” isentropic coordinates (e.g. Yamada and Pauluis, 2016).

>Show obs of [EP flux] vectors with divergence contours. Can the problem be visualized in theta coordinates? The meridional cells look quite different. Presumably the eddy fluxes are similar in both coordinates? Start with Johnson (1989, review). However the Yamada and Pauluis (2016) provides a nice road map for dry and moist isentropic views. Also links to EP flux<

6.4 Summary of Zonal Average Momentum Flow

>describe and show the momentum flow schematic<

The zonal momentum equation in Cartesian coordinates with elevation as the vertical coordinate can be written:

$$\frac{\partial u}{\partial t}+u\frac{\partial u}{\partial x}+v\frac{\partial u}{\partial y}+w\frac{\partial u}{\partial z}-f[v]+\frac{1}{\rho}\frac{\partial p}{\partial x}=F_x \tag{6.44}$$

Using the continuity equation to obtain the flux form and the Bousinesq approximation, then (6.44) can be written (following Lindzen, 1970) as:

$$\frac{\partial u}{\partial t}+\frac{\partial uu}{\partial x}+\frac{\partial uv}{\partial y}+\frac{\partial uw}{\partial z}-fv+\frac{\partial G}{\partial x}=F_x \tag{6.45}$$

Here, G is variable being temporarily defined as $G=\delta p/\rho_0$ where δp is the departure from the hydrostatic value associated with the density ρ_0. Applying a "zonal" average in x (and ignoring any mountain torque type term) yields:

$$\frac{\partial[u]}{\partial t}+[v]\frac{\partial[u]}{\partial y}+[w]\frac{\partial[u]}{\partial z}-f[v]\ =-\frac{\partial[u'v']}{\partial y}-\frac{\partial[u'w']}{\partial z}+[F_x] \tag{6.46}$$

At least away from the equator and for the large scales discussed in this book, it is reasonable to expect thermal wind shear balance to hold. That balance is a combination of hydrostatic and geostrophic balance with the ideal gas law. One can imagine how MMC motions [v] and [w] might interact with eddy fluxes through thermal wind shear balance. Equation (6.46) indicates (as noted above) that convergence and divergence of eddy momentum fluxes would accelerate or decelerate, respectively, zonal mean zonal wind [u]. Where meridional motions [v] have opposite directions in upper versus lower troposphere, conservation of angular momentum during such motions would cause a change in the vertical shear of [u]. Such differential motions of [v] occur in the MMCs. These variables are already visible in (6.46). However, changing the [u] wind shear implies changing the meridional temperature gradient. Additionally, the converse argument holds: eddy heat fluxes that reduce a meridional temperature gradient imply, from thermal wind shear balance, a reduction in the vertical shear of [u]. Furthermore, MMC vertical motions, [w], will change the temperature structure by adiabatic warming or cooling. Since MMCs have net vertical motions that differ between higher and lower latitudes, the meridional temperature gradient is also changed by [w]. So clearly the thermal and momentum field variables are linked, especially where geostrophic balance is important. Therefore, it is

instructive to consider including the eddy heat fluxes into the tendency equation for [u]. A way to include those heat fluxes is by "adding zero" to (6.46); namely by adding and subtracting the same term. After making new combinations of terms, something remarkable happens as one of those combinations is zero (within certain assumptions). Also remarkable, even deeper dynamics are revealed by this action.

The discussion here follows Andrews and McIntyre (1976) for large scale waves who in turn followed a path by Eliassen and Palm (1961) an original study in the context of mountain waves. The discussion above is simple physical reasoning to show an intuitive linkage between zonal momentum tendency and eddy heat flux, the analysis is not limited to where geostrophic balance holds.

Add

$$-\left(\frac{\partial[u]}{\partial y}-f\right)\frac{\partial}{\partial z}\left\{\frac{[v'\theta']}{\frac{\partial[\theta]}{\partial z}}\right\}+\frac{\partial[u]}{\partial z}\frac{\partial}{\partial y}\left\{\frac{[v'\theta']}{\frac{\partial[\theta]}{\partial z}}\right\} \qquad (6.47)$$

to both sides of (6.46). On the LHS combine the first half of (6.47) with the meridional advection and the second half to the vertical advection. The result is:

$$\frac{\partial[u]}{\partial t}+[v^*]\left\{\frac{\partial[u]}{\partial y}-f\right\}+[w^*]\frac{\partial[u]}{\partial z}=-\frac{\partial[u'v']}{\partial y}-\frac{\partial[u'w']}{\partial z}-\left(\frac{\partial[u]}{\partial y}-f\right)\frac{\partial}{\partial z}\left\{\frac{[v'\theta']}{\frac{\partial[\theta]}{\partial z}}\right\}+\frac{\partial[u]}{\partial z}\frac{\partial}{\partial y}\left\{\frac{[v'\theta']}{\frac{\partial[\theta]}{\partial z}}\right\}+[F_x]$$

(6.48)

Here the asterisks denote a "residual circulation" defined by that incorporation of (6.47), namely:

$$\left[v^*\right] = \left[v\right] - \frac{\partial}{\partial z}\left\{\frac{\left[v'\theta'\right]}{\frac{\partial\left[\theta\right]}{\partial z}}\right\}$$

and (6.49)

$$\left[w^*\right] = \left[w\right] + \frac{\partial}{\partial y}\left\{\frac{\left[v'\theta'\right]}{\frac{\partial\left[\theta\right]}{\partial z}}\right\}$$

Following Andrews and McIntyre, we define a temporary vector **G** in the (y, z) plane:

$$\vec{G} \equiv \left\{G_y, G_z\right\} = \left\{\left[u'v'\right] - \frac{\left[v'\theta'\right]}{\frac{\partial\left[\theta\right]}{\partial z}}\frac{\partial\left[u\right]}{\partial z},\ \left[u'w'\right] + \frac{\left[v'\theta'\right]}{\frac{\partial\left[\theta\right]}{\partial z}}\left\{\frac{\partial\left[u\right]}{\partial y} - f\right\}\right\} \tag{6.50}$$

One can rewrite (6.48) using (6.50) as:

$$\frac{\partial[u]}{\partial t} + [v^*]\left\{\frac{\partial[u]}{\partial y} - f\right\} + [w^*]\frac{\partial[u]}{\partial z} = -\frac{\partial G_y}{\partial y} - \frac{\partial G_z}{\partial z} + [F_x] \tag{6.51}$$

For steady, conservative, linear waves, Andrews and McIntyre obtain the result from Eliassen and Palm (1961) that the divergence of G on the RHS of (6.51) is zero; it is sometimes called a "generalized Eliassen-Palm relation".

It is useful to examine how the zonal momentum equation looks when the quasi-geostrophic approximation is applied.

$$\frac{\partial[u]}{\partial t} + [v]\frac{\partial[u]}{\partial y} - f[v] = -\frac{\partial[u'v']}{\partial y} + [F_x] \tag{6.52}$$

Adding

To both sides of (6.52) obtains:

Include something about correlation with [u] tendency mentioned by Pfeffer for .

Got to HERE*

The zonal momentum equation in Cartesian coordinates with pressure as the vertical coordinate can be formed by substituting (C.19) and (C.23) into (C.26). The result is similar to (6.25). After applying a zonal average and dropping the mountain torque term, one obtains:

$$\frac{\partial}{\partial t}[u]+\frac{\partial}{\partial y}[uv]+\frac{\partial}{\partial p}[uw]-f[v]=F_x \tag{6.53}$$

where F_x represents friction in the zonal direction. The nonlinear terms are partitioned into zonal mean and eddy contributions.

$$\frac{\partial}{\partial t}[u]+\frac{\partial}{\partial y}([u][v])+\frac{\partial}{\partial p}([u][\omega])=f[v]-\frac{\partial}{\partial y}[u'v']-\frac{\partial}{\partial p}[u'\omega']+F_x \tag{6.54}$$

A stream function is introduced for the two-dimensional flow in the meridional plane:

$$[v]=\frac{\partial \psi}{\partial p} \quad \text{and} \quad [\omega]=-\frac{\partial \psi}{\partial y} \tag{6.55}$$

Substituting (6.55) into (6.54) and neglecting all terms involving ω obtains:

$$\frac{\partial}{\partial t}[u]+\frac{\partial}{\partial y}([u]\frac{\partial \psi}{\partial p})=f\frac{\partial \psi}{\partial p}-\frac{\partial}{\partial y}[u'v']+F_x \tag{6.56}$$

Expanding the total derivative in the thermodynamic equation (C.3), writing the wind and potential temperature as zonal mean and eddy parts, and applying a zonal average obtains

$$\frac{\partial}{\partial t}[\theta]+\frac{\partial}{\partial y}([v][\theta])+\frac{\partial}{\partial p}([\omega][\theta])=-\frac{\partial}{\partial y}[v'\theta']-\frac{\partial}{\partial p}[\omega'\theta']+\dot{\theta} \tag{6.57}$$

where $\dot{\theta}$ is a diabatic heating rate.

Several simplifying assumptions are applied to the θ equation (6.57). In the quasi-geostrophic system the term involving ω' is neglected in favor of the term involving $[\omega]$ since the zonal average static stability is large enough to make that term comparable to horizontal advection. Other assumptions are: steady motions ($\partial/\partial t = 0$), adiabatic conditions ($\dot{\theta}=0$), and that the zonal mean basic state velocity is $[u]$ only.

********* got to here ******

ℱℱ After showing link to du/dt, show link (in midlats) of del dot F to resid circulation to make that connection. To do that you need to neglect friction and the time

tendency of u in the zonal eqn and then get an approximation that v* relates to minus del dot F. That gets you poleward residual circulation at high levels (400 to 300 mb especially) of the midlats and equatorward motion at very low troposphere (900 mb and below) levels during winter. During NH summer, the del dot F is too weak in the "free troposphere". So, this approximation is a cute aside along the way but not the full residual circulation in practice, which looks more like the isentropic MMC. See "general circulation" section in Edmon et al. (1980).

The last assumption means that since the mean flow has no $[v]$ and $[\omega]$, these motions are only due to the Stokes drift. A subscript s designates the Stokes velocities. Of course, this last assumption also provides a built-in connection between the Stokes drift and the mean meridional circulations derived in §6.3 in addition to the circulation discussed in §6.2.4. Combining the continuity equation for the Stokes motion with the assumptions stated above yields

$$[v]_s \frac{\partial[\theta]}{\partial y} + [\omega]_s \frac{\partial[\theta]}{\partial p} = -\frac{\partial}{\partial y}[v'\theta'] \qquad (7.75a)$$

$$[\omega]_s = -\left(\frac{\partial[\theta]}{\partial p}\right)^{-1} + \frac{\partial}{\partial y}[v'\theta'] \qquad (7.75b)$$

A stream function ψ_s may be defined for the Stokes motion, similar to (7.68). Assuming that the meridional and pressure derivatives of ψ_s are comparable (e.g., as in Figure 6.12a), then the $[v]_s$ term in (7.75a) can be neglected if the surfaces of $[\theta]$ are assumed to be nearly horizontal. The same assumption equates the right-hand side of (7.75b) with a term in (7.74). In order to satisfy a continuity equation for Stokes flow, the heat flux term in (7.73) corresponds to $[v]_s$.

In deriving (7.75), a key assumption is that there be no change in the $[\theta]$ field. This means that any eddy heat flux convergences that attempt to change $[\theta]$ must be cancelled by the mean meridional circulation, ($[v]$, $[\omega]$). By (7.73) and (7.74) the changes to $[\theta]$ caused by the eddy heat fluxes can be thought of as "advection" by the Stokes flow. One could visualize the Stokes flow as attempting to flatten the $[\theta]$ isentropes in the same way that eddy heat fluxes would. To counteract this change, the mean meridional circulation ($[v]$, $[\omega]$) must deform the isentropes in the opposite direction. Two examples illustrate the point.

At this stage a transformed velocity field is introduced

$$v^\natural = [v] - \frac{\partial}{\partial p}\left(\frac{[v'\theta']}{\frac{\partial [\theta]}{\partial p}}\right) \quad (7.73)$$

$$\omega^\natural = [\omega] - \frac{\partial}{\partial y}\left(\frac{[v'\theta']}{\frac{\partial [\theta]}{\partial p}}\right) \quad (7.74)$$

These transformed velocities may seem peculiar at first glance. In actuality, they are the Lagrangian motion of parcels in the meridional plane. The velocities expressed as heat flux terms approximate the "Stokes drift" associated with motions around latitudinally and vertically varying waves. The particular form here is based on Lagrangian motion in the $[\theta]$ equation for small amplitude perturbations.

The *quasi-geostrophic* definition of the EP flux is that $\Upsilon = (\Upsilon^y, \Upsilon^p)$ where the components are defined as

$$(F^y, F^p) = \left(-[u'v'], \frac{f[v'\theta']}{\frac{\partial [\theta]}{\partial p}}\right) \quad (7.66)$$

On a "β-plane" (where f is a linear function of latitude), Υ^y is proportional to the momentum flux and Υ^p is proportional to the heat flux divided by a measure of static stability. Andrews and McIntyre (1976) and Boyd (1976) extend Υ to spherical geometry. Eliassen and Palm (1961) express Υ for an "ageostrophic" case, as do Andrews and McIntyre (1978). The so-called "EP Theorem" states that the divergence of Υ is zero for steady conservative wavelike disturbances upon a zonal wind, or that $\nabla \cdot \Upsilon = 0$. The nondivergence can be shown to apply for certain special conditions.

Profiles of Υ can relate interaction between eddies and a zonal mean state. Edmon et al. (1980) sketch a couple of illustrations of this interaction.

Writing (7.69) as

$$\frac{\partial [u]}{\partial t} + \frac{\partial}{\partial y}\left([u]\frac{\partial \psi}{\partial p}\right) = fv^\natural + \nabla \cdot \mathbf{F} + R \quad (7.76)$$

$$\frac{\partial [u]}{\partial t} + \frac{\partial}{\partial y}\left([u]\frac{\partial \psi}{\partial p}\right) = fv^\natural + \nabla \cdot \Upsilon + F_x \quad (6.58)$$

the quasi-geostrophic form of (7.76), where advecting velocities are geostrophic, leading to $[v] = 0$ once again. Then

$$\frac{\partial [u]}{\partial t} = f[v]_s + \nabla \cdot \mathbf{F} + R$$

where (7.73) has been used. It is clear from this equation that part of the EP flux divergence will be cancelled by the Stokes drift. The cancellation should be obvious immediately since heat fluxes do not appear in the zonal momentum equation!

the EP flux relates to the concept of potential vorticity. For adiabatic motion the Ertel potential vorticity is a conserved quantity. That is,

$$\frac{d}{dt}\left(\frac{\zeta + f}{\frac{\partial P}{\partial \theta}} \right) = 0$$

where the Ertel potential vorticity is the quantity inside the parentheses, and ζ is the relative vorticity normal to a θ surface. (Definitions in other coordinates may be found in Pedlosky, 1987, pp. 38–42.) For quasi-geostrophic motion a similar quantity can be defined from the vertical component vorticity equation (to first order in the Rossby number).

$$\frac{d}{dt}(\zeta + f) = f\frac{\partial \omega}{\partial p} \qquad (7.83)$$

A nondimensional form of the vorticity equation is used here. The adiabatic equation is

$$\omega = \frac{-1}{S}\frac{d\theta}{dt} \qquad (7.84)$$

where $S = [\partial\theta/\partial p]$ is the average pressure derivative of potential temperature. Consistent with the quasi-geostrophic approximation, one assumes that S is a constant. Thus (7.84) is analogous to (7.8), used earlier. If one differentiates (7.84) with respect to pressure and substitutes the result into (7.83), then to first order,

$$\frac{dq}{dt} \equiv \frac{d}{dt}\left(\zeta + f\left(1 + \frac{\partial}{\partial p}\left\{ \frac{\theta}{S} \right\} \right) \right) = 0 \qquad (7.85)$$

This form of the potential vorticity equation is analogous to (7.1), and quasigeostrophic potential vorticity q is again conserved.

One can separate q into zonal mean and eddy parts

$$q = [q] + q'$$

The zonal mean part includes the planetary vorticity, leaving

$$q' = \frac{\partial v'}{\partial x} - \frac{\partial u'}{\partial y} + f\frac{\partial}{\partial p}\left(\frac{\theta'}{S} \right) \qquad (7.86)$$

From this equation it is straightforward to show that the divergence of **F** equals the northward flux of q'.

Multiplying (7.86) by v' and using the chain rule,

$$v'q' = \frac{1}{2}\frac{\partial}{\partial x}\left((v')^2\right) - \frac{\partial}{\partial y}(u'v') + u'\frac{\partial v'}{\partial y} + \frac{f}{S}\left(\frac{\partial}{\partial p}(v'\theta') - \theta'\frac{\partial v'}{\partial p}\right) \qquad (7.87)$$

The perturbation velocities are geostrophic and thus are nondivergent; they also satisfy the nondimensional thermal wind relation.

$$\frac{\partial u'}{\partial x} + \frac{\partial v'}{\partial y} = 0 \quad \text{and} \quad \frac{\partial v'}{\partial p} + \frac{\partial \theta'}{\partial x} = 0 \qquad (7.88)$$

Therefore (7.87) becomes

$$v'q' = \frac{1}{2}\frac{\partial}{\partial x}\left((v')^2\right) - \frac{\partial}{\partial y}(u'v') - \frac{1}{2}\frac{\partial}{\partial x}\left((u')^2\right) + \frac{f}{S}\left(\frac{\partial}{\partial p}(v'\theta') - \frac{1}{2}\frac{\partial}{\partial x}\left((\theta')^2\right)\right)$$

Taking a zonal average around a latitude circle causes the x derivative terms to vanish leaving

$$[v'q'] = -\frac{\partial}{\partial y}[u'v'] + \frac{f}{S}\frac{\partial}{\partial p}[v'\theta'] \equiv \nabla \cdot \mathbf{F} \qquad (7.89)$$

Dickinson (1969) shows that the zonal mean flow can be related to the eddies by the following argument. One writes (7.85) in flux form and applies the zonal average. The x derivatives vanish because the integration is around a closed latitude circle. Since (7.85) is for the quasi-geostrophic system, the advecting velocities are geostrophic, hence $[v] = 0$.

$$\frac{\partial [q]}{\partial t} + \frac{\partial}{\partial y}[v'q'] = 0$$

Differentiating with respect to y yields

$$-\frac{\partial^2 [q]}{\partial t \partial y} = \frac{\partial^2}{\partial y^2}[v'q'] \qquad (7.90)$$

From (7.86) and (7.85) one may write

$$-\frac{\partial [q]}{\partial y} = \mathbf{L}^{\star}[u] \qquad (7.91)$$

where $\mathbf{L}^{\star} = C\partial^2/\partial p^2 + \partial^2/\partial y^2$ and C is a constant. Therefore (7.90), (7.91) and (7.89) are related as follows

$$\frac{\partial \mathbf{L}^{\star}[u]}{\partial t} = \frac{-\partial^2 [q]}{\partial t \partial y} = \frac{\partial^2}{\partial y^2}[v'q'] = \frac{\partial^2}{\partial y^2}(\nabla \cdot \mathbf{F}) \qquad (7.92)$$

One might be tempted to assume that the pressure derivatives in $\mathbf{L}^{\star}$ can be neglected, in which case the divergence of the EP flux will increase $[u]$ up to integrative constants. However, that assumption is misleading (Pfeffer, 1987). One can get a sense for the problems by examining the quasi-geostrophic form of (7.76), where advecting velocities are geostrophic, leading to $[v] = 0$ once again. Then

$$\frac{\partial [u]}{\partial t} = f[v]_s + \nabla \cdot \mathbf{F} + R$$

where (7.73) has been used. It is clear from this equation that part of the EP flux divergence will be cancelled by the Stokes drift. The cancellation should be obvious immediately since heat fluxes do not appear in the zonal momentum equation! Pfeffer (1987) shows that the first two terms on the right-hand side are large, but nearly cancel. In order to eliminate the explicit dependence on $[v]_s$, one obtains the more complicated operator in (7.92). The sensitivity of the operator $\mathbf{L}^{\star}$ is discussed in Pfeffer (1987). For the general case (spherical geometry and variable S) $\mathbf{L}^{\star}$ has variable coefficients. Pfeffer shows that the local derivative of $[u]$ depends strongly on the vertical pattern of the right-hand side of (7.92) and not on the local value of $\nabla \cdot \mathbf{F}$, especially in the higher latitudes of the troposphere. The sensitivity arises from C, which is inversely dependent on static stability S. S is small in the troposphere. That sensitivity probably explains why $\nabla \cdot \mathbf{F}$ and $\partial [u]/\partial t$ are not highly correlated in the troposphere. Baldwin et al. (1985) find the average correlations to be 0.34 in the upper troposphere of the Northern Hemisphere middle latitudes during a winter period. In Hartmann et al. (1984), the best correlations are in the middle stratosphere and near the tropopause; only a few grid points exceed 0.6. In the stratosphere, S is much larger, and one is further away from the surface boundary, so the EP flux divergence method works better; more details are given in §7.4.6. In the troposphere, Pfeffer shows that the traditional reliance upon eddy momentum convergence is a better way to diagnose eddy changes

to the zonal mean flow. What one can conclude about (7.92) is that it is necessary for the eddies to transport potential vorticity in order for them to alter the zonal mean zonal flow.

>>Discuss (above?) why and where EP flux is useful. What not to be misled<<

<GOT TO HERE>

Kuroda 2016, 2017 papers: the subtropical jet, at least in winter (when the H cell is strongest) can be driven by the H cell (the original thinking). While this newer thinking suggests eddies, namely the stationary waves drive the zonal mean jet, and maybe transient eddies as well, the separation is not full. The eddies themselves help drive the MMCs by their eddy covariances (heat and momentum fluxes) so MMCs are still in the picture, we just need to think of them as being driven by more than the diabatic heating. So... **maybe this discussion of jet streams needs to come *after* the K-E equation**. **Placed in chapter 8**. Maybe start by saying that a prominent feature of the zonal momentum is the subtropical jet; that one might think of this jet as flowing from the MMCs since (at least in winter, when the H cell is strongest) the SJ is located at the polar end of the H cell. One can find reduced-complexity models (see list in Kuroda) that examine this link. However, we have seen eddy momentum fluxes being prominent in middle latitudes and it is natural to wonder how they impact the subtropical jet. Do transient eddies only extract energy? With the zonal variations of the SJ being part of the stationary eddy pattern? Or do eddies help maintain it. Certainly our Gill equation sees an indirect role for eddies as they eddy momentum fluxes force the MMC which in turn forces an SJ by angular momentum conservation (if nothing else). But there is "other else". The next chapter considers potential energy and thus heat and temperature so heat and temperature fluxes also play a role in the MMCs and in the SJ. To explore that we need to re-examine those eddy heat fluxes. So, as a bridge to the next chapter, we bring in heat fluxes by first describing the EP fluxes, then seeing how they relate to zonal mean zonal momentum tendency and finally to how the SJ jets may be

linked to MMC and eddy forcing. Either this goes here as a bridge, or it follows the K-E eqn in chapter 8.

A momentum-driving mean meridional circulation (Gill's) and subtropical jet? so that is the next section or the next chapter?? Momentum conservation and jet stream winds/accel from a stop, etc. but that is already in Jeffreys' eqn. Should consider discussing the subtropical (MMC-driven) jet versus the "eddy-driven" jet. **What background is needed for that?** – apparently it needs Kuo-Eliassen, Kuroda-type analysis, so, maybe not here. However, EP fluxes are commonly used to diagnose the maintenance, so does it make sense to introduce them here? Could they be a segue? -- to set up the next chapter which considers potential and total energy?

6.3 Momentum in isentropic coordinates?

The last subsection takes one view of the MMC. However, the MMC looks different in isentropic and equivalent-potential temperature coordinates. A brief introduction to the Eliassen-Palm flux (E-P flux) leads off the discussion.
Kanno & Iwasaki (2018)?

6.3.1 *Eliassen-Palm flux introduction*

>Maybe introduce the EP flux link to momentum and vorticity here? Start with 7.4.1-7.4.3 in original book. This includes a meridional cell discussion that links heat fluxes as well as momentum, so it builds on Gill's eqn. in immediate prior sub-section. Use that to launch into the Karoda papers and then a discussion of MMC-driven and eddy-driven jets. <

See Kuroda papers (2016 and 2017) for NHem and SHem respective winter subtropical jets – these use EP fluxes which should be introduced first. They also provide a concise list of papers relating to eddy driven versus pure AAM conservation descriptions.

It is easy to emphasize the subtropical jets since they are maxima in the zonal mean zonal momentum. The tropics have easterlies and seasonal reversals; Dima et al. (2005) have some discussion (but check if that is post or pre eddy-driven jets). Yang et al. (2013) cite Dima et al. show how the zonal momentum balance differs inside and outside the Asian monsoon region. Kuroda 2016 also cites Dima et al. Caballero (2007) discusses eddy impacts on the H cell including the first order momentum balance between acceleration by meridional flux of absolute vorticity and deceleration by zonal mean of eddy momentum divergence ($u'v'$).

>follow Gill's eqn<

>Also refer back to the mean meridional cells in fig 6.9 (term c?) captured by the Coriolis term.

6.3.2 *Dry and moist isentropic views of momentum balance*

>Can the problem be visualized in theta coordinates? The meridional cells look quite different. Presumably the eddy fluxes are similar in both coordinates? Start with Johnson (1989, review). However the Yamada and Pauluis (2016) provides a nice road map for dry and moist isentropic views. Also links to EP flux<

6.4 Summary of Zonal Average Momentum Flow

>describe and show the momentum flow schematic<

GOT TO HERE

<GOT TO HERE>

~~6.5 Vorticity dynamics: Rossby wave source (Vorticity tendency, heating and cooling specified – in Chap 8?)/ former 6.5 – but that is in the Chap 9 list of how do tropics/extrop interact?) reconcilliation of mom flx & jet position?? But already have Newton's fig 9.8 matching KE tendencies above or below? But that fig uses KE tendency. Discuss vorticity eqn for developing frontal cyclones? – no, that is useful to debunk nonmodal growth. Could~~

~~**do QGPV cons and topographic-generated waves – but keep as input into long waves generation question in Chapter 9**~~

~~.What stationary wave causes that negative max straddling the equator in the eastern Pacific?~~

~~Discuss the SHem in DJF What type of transient causes that equatorial max in the SHem? Must be the SPCZ changes~~

~~Discuss the NHem and SHem in JJA~~

Chapter 7 Energetics

7.1 Overview and context of this chapter. (Motion and temperature in an Energetics context?)

7.2 **Kinetic energy and its components**

A natural extension of the angular momentum concepts presented in the previous section is the analysis of kinetic energy. The total kinetic energy can be partitioned into contributions by the zonal mean flow and by the zonally varying flow. Horizontal component expressions for the zonal average kinetic energy ($K_Z = \{K_Z^x, K_Z^y\}$) are derived first. Then the horizontal total kinetic energy component equations ($K_H = \{K^x, K^y\}$) are derived. The eddy kinetic energy ($K_E = \{K_E^x, K_E^y\}$) is simply the difference between the other energy components:

$$\begin{aligned} K^x &= K_Z^x + K_E^x \\ K^y &= K_Z^y + K_E^y \\ K_H &= K_Z + K_E \end{aligned} \qquad (4.10)$$

The subscript Z refers to the kinetic energy of the zonal average flow. The subscript "E" refers to the kinetic energy of the deviations from the zonal mean flow, i.e., from the eddies. The zonal mean of an eddy quantity is zero. The energies here are defined with volume averages. The zonal average part of the volume average eliminates all cross products between eddy and zonal mean quantities (see Appendix; e.g., $u'[u]$ terms vanish).

$$\begin{aligned} K_H &= \int_V \left(\frac{[uu]+[vv]}{2} \right) \rho dxdydz \\ &= \int_V \left(\frac{[u]^2}{2} + \frac{[v]^2}{2} \right) \rho dxdydz + \int_V \left(\frac{[u'^2]}{2} + \frac{[v'^2]}{2} \right) \rho dxdydz \end{aligned} \qquad (4.11)$$

The inclusion of density in (4.8) gives kinetic energy densities; the integrals are thus over the mass within a given volume.

4.2.1 *Derivations*

The equations for K_Z are derived first. The longitudinal (brackets) average of the horizontal equations of motion are taken. (This step parallels eqs. 2.19 and 2.20 in Holton, 1979, except using pressure as the vertical coordinate.) The u equation (in flux form) is multiplied by $[u]$ and the v equation (also in flux form) by $[v]$. Bringing the brackets term inside the time derivative obtains:

$$\frac{\partial}{\partial t}\left(\frac{[u]^2}{2}\right)+\frac{[u]}{R}\frac{\partial R[uv]}{\partial y}+[u]\frac{\partial[u\omega]}{\partial P}-\frac{[u][uv]\tan\phi}{r}$$
$$-f[u][v]+[u][F_x]=0$$
$$\frac{\partial}{\partial t}\left(\frac{[v]^2}{2}\right)+\frac{[u]}{R}\frac{\partial R[vv]}{\partial y}+[\upsilon]\frac{\partial[u\omega]}{\partial P}-\frac{[v][uu]\tan\phi}{r}$$
$$+f[u][v]+[v][F_y]+g[v]\frac{\partial[z]}{\partial y}=0$$

The pressure gradient term integrates out of the $[u]$ equation if mountain torque is neglected. That assumption is made here on the basis that zonal mountain torque could be parameterized by modifying the F_x friction term. Also, $dy = rd\phi$ where ϕ is latitude and r is the earth's radius. Two terms may be combined:

$$\frac{[u]}{R}\frac{\partial R[uv]}{\partial y}-\frac{[u][uv]\tan\phi}{r}\equiv\frac{[u]}{R^2}\left(\frac{\partial R^2[uv]}{\partial y}\right)$$

Integrating the $K^x{}_Z$ and $K^y{}_Z$ equations over the mass of the fluid gives:

$$\frac{\partial}{\partial t}\int\underbrace{\left(\frac{[u]^2}{2}\right)}_{(A)}dm+\int\underbrace{\left(\frac{[u]}{R}\right)}_{(B)}\underbrace{\left(\frac{1}{R}\frac{\partial R^2[uv]}{\partial y}+\frac{\partial R[u\omega]}{\partial P}\right)}_{(C)}dm$$
$$-\int f[u][v]dm+\int[u][F_x]dm=0 \qquad (4.12)$$

The integrand *(A)* is K_Z^x as in (4.10).

$$\frac{\partial}{\partial t}\int\underbrace{\left(\frac{[v]^2}{2}\right)}_{(D)}dm+\int[v]\underbrace{\left(\frac{1}{R}\frac{\partial R^2[vv]}{\partial y}+\frac{\partial[v\omega]}{\partial P}\right)}_{(E)}dm$$
$$+\int\frac{[v][uv]\tan\phi}{r}dm+\int\underbrace{g[v]\frac{\partial[z]}{\partial y}}_{G}dm \qquad (4.13)$$
$$+\int f[u][v]dm+\int[v][F_y]dm=0$$

The integrand (D) is K_Z^y as in (4.10). Parts (B) and (C) have an *angular* weighting by R. Term (E) does not have the R weighting as in (B) because the tan ϕ term has not been incorporated into (E). Term (G) is a pressure work term.

The Coriolis term appears in both (4.12) and (4.13), but it is merely acting to exchange energy between those components. The Coriolis force terms cancel when (4.12) and (4.13) are summed. They must cancel since the rotation of the earth cannot be a source of energy to the atmosphere. Upon integrating (4.12) over the mass of the atmosphere, the second term can be expanded:

$$\int \frac{[u]}{R}\left(\frac{1}{R}\frac{\partial R^2[uv]}{\partial y}+\frac{\partial R[u\omega]}{\partial P}\right)dm \equiv \int\left(\frac{1}{R}\frac{\partial R[u][uv]}{\partial y}+\frac{\partial [u][u\omega]}{\partial P}\right)$$
$$dm-\int\left([Ruv]\frac{\partial}{\partial y}(\frac{[u]}{R})+[Ru\omega]\frac{\partial}{\partial P}(\frac{[u]}{R})\right)dm \qquad (4.14)$$

If the integration is over the whole atmosphere (a closed system), then the first right-hand side integral in (4.14) is zero since the integrand contains two perfect differentials. The $1/R$ term vanishes since $dm = -grRdpd\phi d\lambda$ where λ is longitude. The kinetic energy equations (4.12) and (4.13) can be interpreted using either side of the expression in (4.14) depending upon which is more convenient. The left-hand side integrand is convergence of relative angular momentum weighted by an angular velocity. The right-hand side is the gradient of an angular velocity weighted by the momentum flux.

The observed vertical distribution of momentum flux looks schematically like Figure 4.5a. The convergence of the flux builds $[u]/R$ westerly momentum. Since this convergence is largest at an upper level, then the jet will be at an upper level (as in the observations; e.g., Figure 3.15). Figure 4.5 is a schematic illustration of the link between convergence and $[u]$. The last integral in (4.14) indicates that to change $[u]/R$, the eddy flux of angular momentum must go up or down the gradient of the angular velocity (up the gradient means from lower to higher values). The last integral in (4.14) equals zero at the maximum angular velocity.

Similarly, for meridional motion the second term in (4.13) can be expanded as

$$\int [v]\left(\frac{1}{R}\frac{\partial R[vv]}{\partial y}+\frac{\partial [v\omega]}{\partial P}\right)dm \equiv \int\left(\frac{1}{R}\frac{\partial R[v][vv]}{\partial y}+\frac{\partial [v][v\omega]}{\partial P}\right)$$
$$dm-\int\left([vv]\frac{\partial [v]}{\partial y}+[v\omega]\frac{\partial [v]}{\partial P}\right)dm \qquad (4.15)$$

The interpretation here is essentially the same as for the $[u]/R$ term just discussed except that the factor of R is missing. A critical distinction here is that the left-hand sides of (4.14) and (4.15) are intuitively useful for understanding local contributions. The right-hand sides are tailored more for a global average description since the first integral on the right-hand side vanishes in that latter case.

The final form of the kinetic energy equation for the zonal mean motions is given by (4.16).

$$\frac{\partial K_Z^x}{\partial t}=\int\left([Ruv]\frac{\partial}{\partial y}\left(\frac{[u]}{R}\right)+[Ru\omega]\frac{\partial}{\partial P}\frac{[u]}{R}\right)dm$$
$$+\int f[u][v]dm-\int[u][F_x]dm=0 \qquad (4.16a)$$
$$\frac{\partial K_Z^y}{\partial t}=\int\left([vv]\frac{\partial [v]}{\partial y}+[Rv\omega]\frac{\partial [v]}{\partial P}\right)dm-\int\frac{[\upsilon][uu]\tan\phi}{r}dm$$

$$-\int g[v]\frac{\partial[z]}{\partial y}dm-\int f[u][v]dm-\int[v][F_y]dm=0 \qquad (4.16b)$$

To derive the *total* kinetic energy equations one multiplies the *u* equation of motion (in advective form) by *u* and the *v* equation by *v*, bringing the terms inside the time integration and then taking the brackets average. The derivation is:

$$\frac{\partial}{\partial t}=\left(\frac{u^2}{2}\right)+\underbrace{u\frac{\partial}{\partial x}\left(\frac{u^2}{2}\right)\frac{v}{R}\frac{\partial}{\partial y}\left(\frac{Ru^2}{2}\right)+\omega\frac{\partial}{\partial P}\left(\frac{u^2}{2}\right)}_{(A)}$$

$$-\frac{u^2v\tan\phi}{r}+gu\frac{\partial z}{\partial x}-fuv+uF_x=0 \qquad (4.17)$$

Term (A) is rearranged by using the continuity equation in pressure coordinates and the chain rule:

$$(A)\frac{\partial}{\partial x}=\left(\frac{uu^2}{2}\right)+\frac{1}{R}\frac{\partial}{\partial y}\left(\frac{Rvu^2}{2}\right)+\frac{\partial}{\partial P}\left(\frac{\omega u^2}{2}\right)$$

The equation is now in flux form. The meridional component kinetic energy is similarly manipulated:

$$\frac{\partial}{\partial t}=\left(\frac{v^2}{2}\right)+\underbrace{u\frac{\partial}{\partial x}\left(\frac{v^2}{2}\right)\frac{v}{R}\frac{\partial}{\partial y}\left(\frac{Rv^2}{2}\right)+\omega\frac{\partial}{\partial P}\left(\frac{v^2}{2}\right)}_{(B)}$$

$$+\frac{u^2v\tan\phi}{r}+gv\frac{\partial z}{\partial y}+fuv+vF_y=0 \qquad (4.18)$$

One notes that

$$(B)\frac{\partial}{\partial x}=\left(\frac{uv^2}{2}\right)+\frac{1}{R}\frac{\partial}{\partial y}\left(\frac{Rvv^2}{2}\right)+\frac{\partial}{\partial P}\left(\frac{\omega v^2}{2}\right)$$

Applying the zonal average yields:

$$\frac{\partial}{\partial t}=\left(\frac{u^2}{2}\right)+\frac{1}{R}\frac{\partial}{\partial y}\left[\frac{Rvu^2}{2}\right]+\frac{\partial}{\partial P}\left[\frac{\omega u^2}{2}\right]$$

$$-\frac{[uuv]\tan\phi}{r}+g[u\frac{\partial z}{\partial x}]-f[uv]+[uF_x]=0$$

$$\frac{\partial}{\partial t}=\left(\frac{v^2}{2}\right)+\frac{1}{R}\frac{\partial}{\partial y}\left[\frac{Rvv^2}{2}\right]+\frac{\partial}{\partial P}\left[\frac{\omega v^2}{2}\right]$$

$$-\frac{[uuv]\tan\phi}{r}+g[u\frac{\partial z}{\partial y}]+f[uv]+[vF_y]=0$$

Integrating over the entire mass of the atmosphere, the second and third terms vanish using $\omega = 0$ at the top and bottom on average. The first terms are just the rate of change of total kinetic energy

$$\frac{\partial K^x}{\partial t} = \int \left(\frac{([uuv]\tan\phi)}{r} + f[uv] \right) dm - \int g \left[\frac{\partial z}{\partial x} \right] - \int [uF_x] dm = 0 \qquad (4.19a)$$

$$\frac{\partial K^y}{\partial t} = -\int \left(\frac{([uuv]\tan\phi)}{r} + f[uv] \right) dm - \int g \left[\frac{\partial z}{\partial y} \right] - \int [vF_y] dm = 0 \qquad (4.19b)$$

The first integral is a conversion between K^x and K^y; it merely states that the Coriolis terms must cancel in the net summation; planetary rotation cannot be a source of energy.

The two equations in (4.19) indicate that the time rate of change of total kinetic energy is due to the work done by pressure forces and the work done by friction.

The component *eddy* kinetic energy equation is derived by subtracting (4.16) from (4.19). Component terms in (4.11) are combined in these steps.

$$\frac{\partial K_E}{\partial t} = -\int [Ruv] \frac{\partial}{\partial y} \left(\frac{[u]}{R} \right) + [Ru\omega] \frac{\partial}{\partial P} \left(\frac{[u]}{R} \right) + [vv] \frac{\partial [v]}{\partial y} + [v\omega] \frac{\partial [v]}{\partial P}$$
$$- \frac{[v][uu]\tan\phi}{r} dm + \int g \left(\left[u' \frac{\partial z'}{\partial x} \right] + \left[v' \frac{\partial z'}{\partial y} \right] \right) dm$$
$$- \int ([u'F_x'] + v'F_y'] dm = 0$$

The first integral converts kinetic energy between zonal and eddy components. The second integral is related to vertical overturnings. A closed system model is used in the section on available potential energy (§4.5.2) to elucidate these overturnings; they are conversions between kinetic and available potential energy. The last integral is frictional extraction.

The five parts of the first integral can be rearranged and combined. For example:

$$[Ru\omega] \frac{\partial}{\partial P} \left(\frac{[u]}{R} \right) = \underbrace{R[u][\omega] \frac{\partial}{\partial P} \left(\frac{[u]}{R} \right)}_{\text{A}} + \underbrace{R[u'\omega'] \frac{\partial}{\partial P} \left(\frac{[u]}{R} \right)}_{\text{B}}$$

R is not a function of P, so it cancels out. Using the chain rule obtains:

$$(A) = [\omega] \frac{\partial}{\partial P} \left(\frac{[u]^2}{R} \right) = \underbrace{\frac{\partial}{\partial P} \left([\omega] \frac{[u]^2}{2} \right)}_{\text{C}} - \underbrace{\left(\frac{[u]^2}{2} \right) \frac{\partial [\omega]}{\partial P}}_{\text{D}}$$

Terms like (B) will contribute to the final K_E equation. Terms like (D) combine and cancel from the continuity equation. Terms like (C) combine to form:

$$\nabla_2 \cdot \left\{ \left(\frac{[u]^2 + [v]^2}{2} \right) [\mathbf{V}_2] \right\} \equiv (E)$$

where $\mathbf{V}_2 = (v, \omega)$ and $\nabla_2 = (\partial/\partial y, \partial/\partial P)$. Term (E) vanishes when integrated over the entire mass of the atmosphere. Term (E) is a two-dimensional perfect differential because longitude was removed from the problem by the brackets average.

When the eddy kinetic energy tendency is integrated over the entire mass of the atmosphere (dm), only squares of the primed quantities are left.

$$\frac{\partial K_E}{\partial t} = -\int \left(\underbrace{[Ru'v']\frac{\partial}{\partial y}\left(\frac{[u]}{R}\right) + [Ru'\omega']\frac{\partial}{\partial P}\left(\frac{[u]}{R}\right)}_{\text{(A)}} + \underbrace{[v'v']\frac{\partial[v]}{\partial y} + [v'\omega']\frac{\partial[v]}{\partial P} - \frac{[v][u'u']}{r}\tan\phi}_{\text{B}} \right) dm \tag{4.20}$$

$$-\int \underbrace{g\left(\left[u'\frac{\partial z'}{\partial x}\right] + \left[v'\frac{\partial z'}{\partial y}\right] \right)}_{\text{C}} dm - \int \underbrace{([u'F_x') + v'F_y']}_{\text{D}}\, dm = 0$$

4.2.2 *Interpretation*

The schematic features of the momentum budget are seen in the following observations. Figure 4.6 shows a calculation of the frictional torque exerted by the atmosphere on the surface of the earth, as determined from surface wind and pressure observations. Oort (1985) also notes that oceans exert a torque upon the solid earth in a manner similar to the atmospheric mountain torque; the dashed line in Figure 4.6 shows this "continental" torque. Negative continental torque is created by sea levels that slope upward from east to west. The atmospheric circulations impart frictional torque onto the oceans, which in turn transfer the torque to the solid earth. Consequently, the two curves in Figure 4.6 are quite similar. Both curves show the *atmosphere* gaining momentum in the tropics and losing momentum in the extratropics. To balance the gains, there must be large poleward transport of absolute angular momentum occurring in the subtropics of both hemispheres. For net balance by the earth, atmosphere, and oceans, the solid earth must transport angular momentum the opposite way. Oort (1985) proposes the controversial notion that the slipping of the crust along properly oriented fault lines could accomplish the task.

The time rate of change of kinetic energy is proportional to friction and to the convergence of momentum fluxes. From (4.14) and (4.15) the latter is proportional to the gradient of momentum transport weighted by the angular velocity. As detailed in the Appendix, many different physical phenomena contribute to a [uv] momentum flux. Figure 4.7 illustrates the relative contributions by several classes of phenomena. The Appendix defines the notation.) The discussion of the observed momentum fluxes' contribution to zonal mean kinetic energy balance proceeds as follows. The fluxes by the mean meridional cells are discussed first, then the eddy fluxes, and finally both circulations are considered together.

4.2.2.1 *Zonal mean cells transport*

The contribution by the mean meridional cells has the opposite sign in the middle latitudes as it does in the tropics (Figure 4.7d). The sign reversal follows from the three-cell description of the mean meridional circulation. ($[u]$ is large and mainly westerly in the upper troposphere; at that altitude $[v]$ is poleward in the subtropics and equatorward in middle latitudes.) As mentioned in §3.3, the Hadley cell is much stronger in the winter hemisphere. The poleward fluxes in the subtropics (Figure 4.7d) reflect that seasonal change.

Figure 4.8 illustrates the vertical variation of the northward momentum flux due to the mean meridional cells. The vertical variation is schematically deduced in Figures 4.8a,b; confirming observations are shown in Figure 4.8c. The Northern Hemisphere Hadley cell has $[v] < 0$ at low levels and $[v] > 0$ in the upper troposphere, where $[u]$ is negative (easterly, shaded in Figure 4.8a). When a vertical average is taken, there is some cancellation, but the low-level contribution is greater in the tropics because $[u]$ is greater at low levels (Figure 3.14). Thus Figure 4.7d shows northward (positive) transport. In the subtropics $[u]$ and $[v]$ are both positive in the upper atmosphere and the vertical average transport is strongly poleward. The Northern Hemisphere Ferrel cell has positive $[v]$ at low levels and negative $[v]$ above, while $[u]$ is positive (westerly) throughout. Again there is some cancellation when a vertical average is taken but the westerlies at the jet stream level are much stronger than the low-level zonal wind. Hence, the vertical average is negative in midlatitudes as seen in Figure 4.7d.

4.2.2.2 *Eddy transports*

(a) Momentum transport by the transient eddies (Figure 4.7b) is much greater than that by the mean meridional circulations. Hence, eddies are the primary mechanism maintaining the zonal mean zonal flow. One could expect this. The velocity in the mean meridional cells ($[v]$) is an order of magnitude smaller than the typical v measured instantaneously at a point. So one anticipates that $[u][v] << [u'v']$, even though $[u]$ is large. (b) Transient eddy transports (Figure 4.7b) are less during summer, especially in the Northern Hemisphere. The eddy transports are greatest at about 30° latitude in both hemispheres. (c) The stationary wave flux (Figure 4.7c) is only significant in the Northern Hemisphere; it is quite large during winter. The standing wave pattern includes poleward transport in midlatitudes and equatorward transport at high latitudes. The former is seen in the characteristic shape of the long wave troughs. Those troughs are often oriented southwest to northeast, an orientation that creates poleward momentum flux (Figures 4.9, 5.9, 6.8, and 6.9). The equatorward momentum flux at high latitudes can be understood from the typical life cycle of the frontal cyclones. As these storms grow, they move poleward as well as eastward. Eventually they often merge with the “semi-permanent” Aleutian and Icelandic Lows. At this point they decay, and one mechanism of decay (barotropic instability) has eddy momentum convergence. That convergence creates equatorward fluxes at high latitudes. (d)

Classical theories about the general circulation (§1.3) completely neglected these eddy fluxes because eddies were not included. Those theories stated that the pressure forces, modified by the Coriolis effect, were the generators of zonal kinetic energy.

Even though the eddy velocities (u', v') have no zonal mean, the product of these velocities can have a nonzero zonal mean if the eddy has a special structure. Schematic diagrams (Figures 4.9 and 4.10) illustrate how the eddy momentum flux can have a zonal average contribution. For circular low and high pressure patterns (Figure 4.10), there is no net contribution to the zonal average eddy momentum flux even though the term may be locally large; the contributions to the zonal average on the east and west sides of the low (or high) cancel. The eddies must have asymmetry (Figure 4.9) to obtain a net zonal average eddy momentum flux. More precisely, there must be horizontal tilts of the trough and ridge axes. The horizontal tilts deform, in effect *rotate*, the location of maximum and minimum $u'v'$. A northwest to southeast tilt will give a southward flux ($u'v' < 0$) in the middle latitudes by rotating the $u'v'$ pattern clockwise. A southwest to northeast tilt will give a northward flux ($u'v' > 0$) by rotating the $u'v'$ pattern in Figure 4.10 counter clockwise. The direction of the flux is understood as an advection of eddy zonal momentum (u') by the eddy meridional velocity (v') in the meridional direction. Hence $u'v' > 0$ can occur with northward advection ($v' > 0$) of positive zonal momentum ($u' > 0$). Equivalently, southward advection ($v' < 0$) of easterly momentum ($u' < 0$) also is a northward flux of westerly zonal momentum. This interpretation follows simply because *the $u'v'$ terms in (4.20) originate from the meridional advection term in the zonal momentum equation*. Zonal averages are fundamental to the discussion here. If these terms were examined for *local* building or damping the jet, then one would need to retrieve the cross-product terms (e.g., $[u]v'$ type terms) that were neglected previously.

The eddy momentum fluxes, like the fluxes from mean meridional cells, are largest near the tropopause level. For the eddies, the maximum transport is located close to the maximum velocity found for the tropospheric jet streams described earlier. Figure 4.11 shows observed annual mean momentum fluxes by all circulations. The maximum transient eddy contribution to the total flux is about 8 to 10 times greater than that by meridional cells or standing eddies. Transient eddy fluxes are shown in Figure 4.12e and f. Inspection of Figures 4.8c, 4.11, and 4.12e and f shows that the Hadley cells reinforce the eddy fluxes but the Ferrel cells oppose the eddy fluxes in midlatitudes. This point is returned to in the theoretical explanation of the Ferrel cell given in §6.3.2.

At this stage some care is needed to account for the *angular* velocity being used. The cosine of latitude in R shifts the location of maximum $[u]/R$ poleward of the climatological jet stream position. Also, the $\cos\phi$ is missing from the numerator of the eddy term displayed in Figure

4.11; correcting for that shifts the eddy momentum flux maximum slightly equatorward. With thes

e adjustments, the momentum transport is directed up the gradient of the angular velocity, at least on the equatorward side of the jet. However, the match between the $[u]/R$ and momentum convergence fields is not exact.

Figure 4.12 shows other observations, based upon diagrams in Newell et al. (1970). R is not included. If one weights the momentum fluxes (Figures 4.12e and f) by $[u]/R$, then the maximum change of the mean kinetic energy will be near the 200 to 300 hPa layer and around 40 N and 30 to 50 S in the respective winter seasons. These resultant locations match the locations of the jet streams better than simply using the momentum convergence. These locations are poleward of where the eddy momentum convergence (a gradient of the quantity diagrammed) is greatest. There are two matters to consider and §6.3 and §6.5 return to this subject. First, the eddy momentum and heat fluxes occur in a way that destroys thermal wind balance. To regain the balance, a Ferrel cell motion is set up that shifts the position of the jet equatorward from the location of maximum momentum convergence (§6.3). Second, Figure 4.10 shows that the subtropical jets seem to lie at the boundary between the Ferrel and Hadley cells. In §6.5 the linkage between jets and meridional cells is shown to more subtle. The full explanation of these mechanisms requires further background and that explanation is left to §6.3 and §6.5.

The discussion so far has centered around the observed sources of the meridional flux of zonal momentum ($[uv]$). This flux is an important element in the maintenance of the zonal mean jet streams. The zonal and eddy kinetic energy can be changed by other processes. The eddy kinetic energy equation (4.20) groups the processes into four categories. The zonal mean kinetic energy equation can be similarly grouped. The four groups in (4.20) are specifically interpreted next.

- *Term (A)* contains fluxes of eddy momentum weighted by the zonal mean angular zonal velocity gradient. Term (A) is a conversion between different forms of kinetic energy; the same term but with opposite sign is found in (4.16).
- *Term (B)* contains fluxes of eddy momentum weighted by the mean meridional velocity gradient. Terms (A) and (B) together are sometimes labelled the “barotropic” energy conversion terms. Since $[v] << [u]$ and $[v' v'] \sim [u' v']$, (B) tends to be smaller than (A). The same term, but with opposite sign, occurs in (4.16).
- *Term (C)* is comprised of work done by pressure forces. The correlations of eddy velocity and eddy pressure gradient are sometimes categorized as “baroclinic” terms. The term is conversion between potential energy and eddy kinetic energy, so a related term is found in the available potential energy equation. To visualize the role played by this term, one must understand the concept of available potential energy. Thus, term (C) is examined in much greater detail in §4.5.2.

- *Term (D)* includes the net loss of kinetic energy due to various frictional processes.

Terms (A) and (B) in (4.20) can either be a source or sink. The variation in the sign of these terms will be described in more detail when baroclinic and barotropic instability theory are considered over limited longitudinal segments. The pressure work terms (C in 4.20) can be a source or a sink as well. The frictional dissipation term (D) is always a sink. It is essentially a leakage of energy down in scale to turbulent length scales.

The subject of angular momentum is returned to in §6.2 when more recent theoretical ideas about the general circulation are discussed. The reader need not complete this chapter in order to follow the discussion in §6.2. This section briefly considered kinetic energy; the next section examines the role and definition of potential energy. After that, the linkage between kinetic and potential energy is considered.

7.3 Potential energy

7.3.1 Dry and moist static energy

Heat fluxes in terms of small diff between large, opposite fluxes? Says something about efficiency which also implies Carnot cycle. **Maybe this belongs at start of the APE discussion**?

7.3.2 APE formulations

7.4 Component (limited volume) energetics

Bring back KE at end as did before?

7.5 Baroclinic and Barotropic Energy Conversions

7.6 Observed heat fluxes

6.4 Momentum and Heat parallel cycles, but this page**:**
http://atm.ucdavis.edu/~grotjahn/course/atm240/momntm.htm

Needs energetics. So, both mom/KE and heat/APE together makes a nice ending.

HOMEWORK problems

1. The global mean *relative* atmospheric angular momentum is about 1.5 x 10^8 J-s.

a. Assuming a simple "solid body" superrotation flow of $u = u_{sbr} \cos\varphi$, find u_s for an isothermal atmosphere at 270K and 10^5 Pa surface pressure on a spherical Earth (i.e. no topography). What is u_{sbr}? Hint: assume hydrostatic conditions and a constant scale height for the vertical integration.

b. Part a) would be unrealistic several ways. One fault is it would speed up the Earth's rotation. To alleviate that fault, simplify the pattern of surface easterlies and westerlies by assuming the zonal wind is zero at the surface. Define crude "midlatitude jet streams" by assuming $u = u_{sj} \sin(\pi p / 10^5) \sin^2(2 \varphi)$. Assume thermodynamic and hydrostatic conditions as in part a.). What is u_{sj}? How does it compare with actual jet stream maxima? How would lowering the latitude of the peak in u change the estimate of u_{sj}? How would moving the jet to a lower pressure change u_{sj}?

2. Solid Earth deceleration example in Egger et al:

To get a feeling for the orders of magnitude involved, let us consider a cubic mountain block of 1000 m height, zonal extension of 100 km, and meridional extent of 1000 km at 45_N. If the surface pressure at the western wall exceeds that in the east by 10 hPa, (20) gives To3 = -4.5 Had. The corresponding deceleration of globally superrotating atmospheric flow is approximately -0.03 m s_1 if the torque acts for 1 d and if there are no mass shifts.

3. base problem on momentum exchanges in atm and ocean, see p. 246 in Peixoto and Oort book.

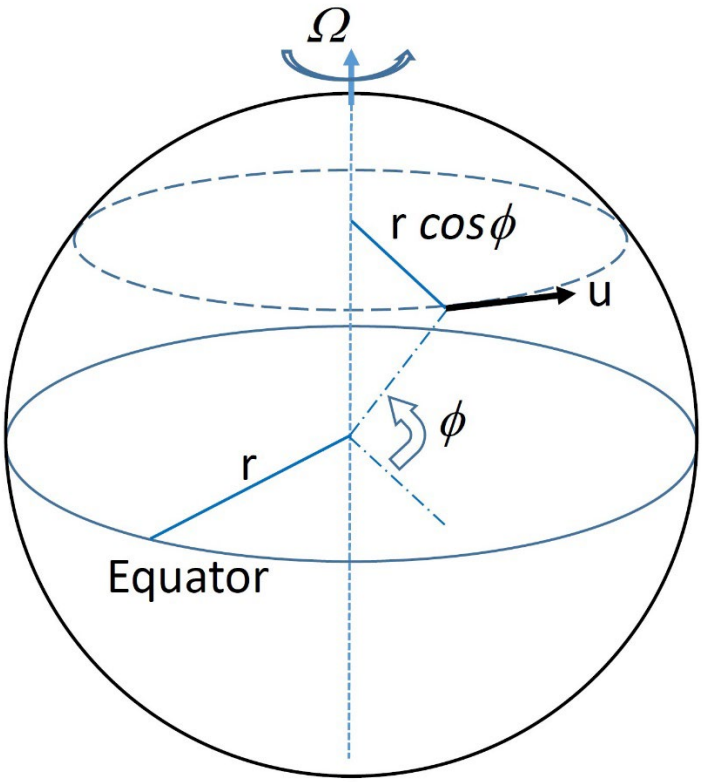

Figure 6.1 Geometry indicating the distance from the axis of rotation ($r\ cos\varphi$) at latitude φ. Assumptions include that the Earth is a sphere and the thickness of the atmosphere can be neglected.

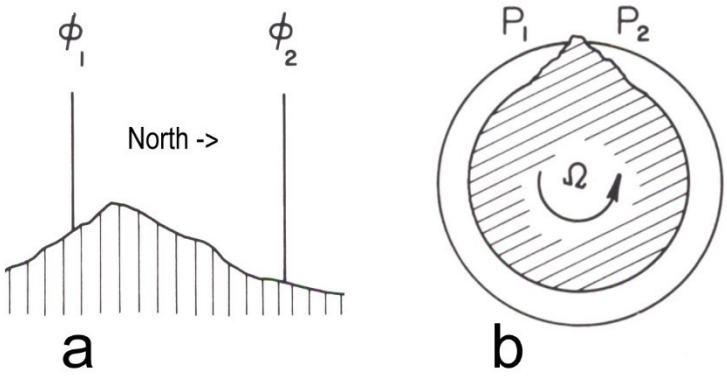

Figure 6.2 Momentum equation schematic geometry. a) Latitudes φ_1 along which surface S_1 is defined and φ_2 along which surface S_2 is defined bound the volume in (6.4) where subscript 1 is South of subscript 2. The bounding integrals in (6.4) have different surface areas due to differing latitudes and topography. b) Orientation of the pressure values p_1 and p_2 in (6.7) where one mountain interrupts the integral around the Earth. More than one topographic feature can interrupt the integral and contribute to the mountain torque term. Longitude increases going counter-clockwise in this view from above the North Pole.

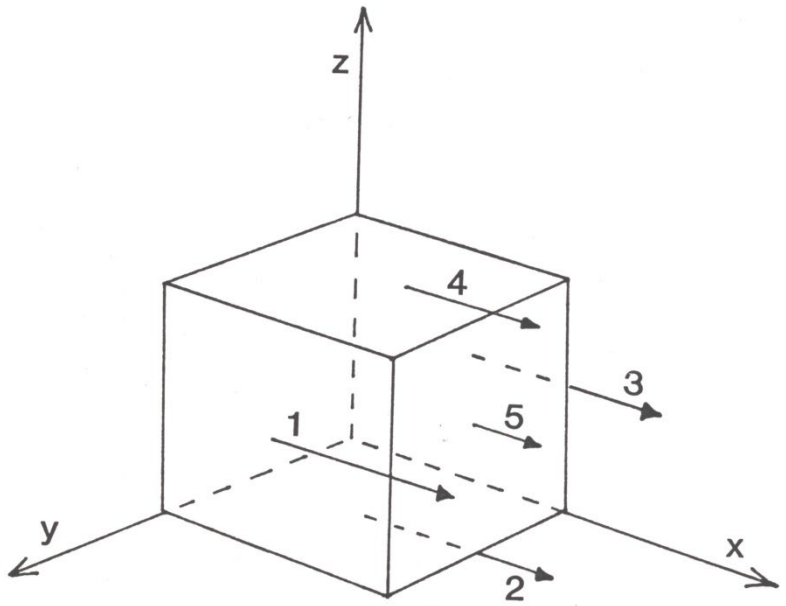

Figure 6.3 Notation for stress tensors in the '*x*' direction. Stress applied along the top and bottom surfaces in the *x* direction, indicated by arrows 4 and 2 contribute to τ_{xz}. A viscous pressure force in the *x* direction is τ_{xx} and labelled arrow 5. Stress tensors in the direction of arrows 1 and 3 contribute to τ_{xy}.

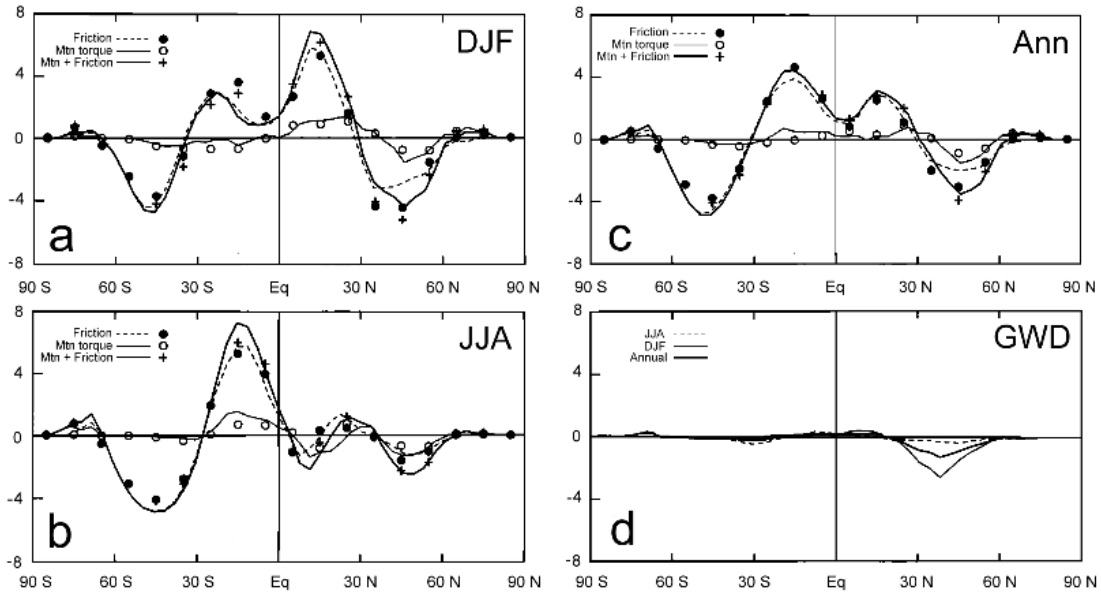

Figure 6.4 a), b) Seasonal …---------- Units are Hadleys per 2.5 degrees latitude. Lines redrawn and rescaled from Huang et al. (1999) including symbols from Newton (1972) to facilitate comparison with Figure 6.5.

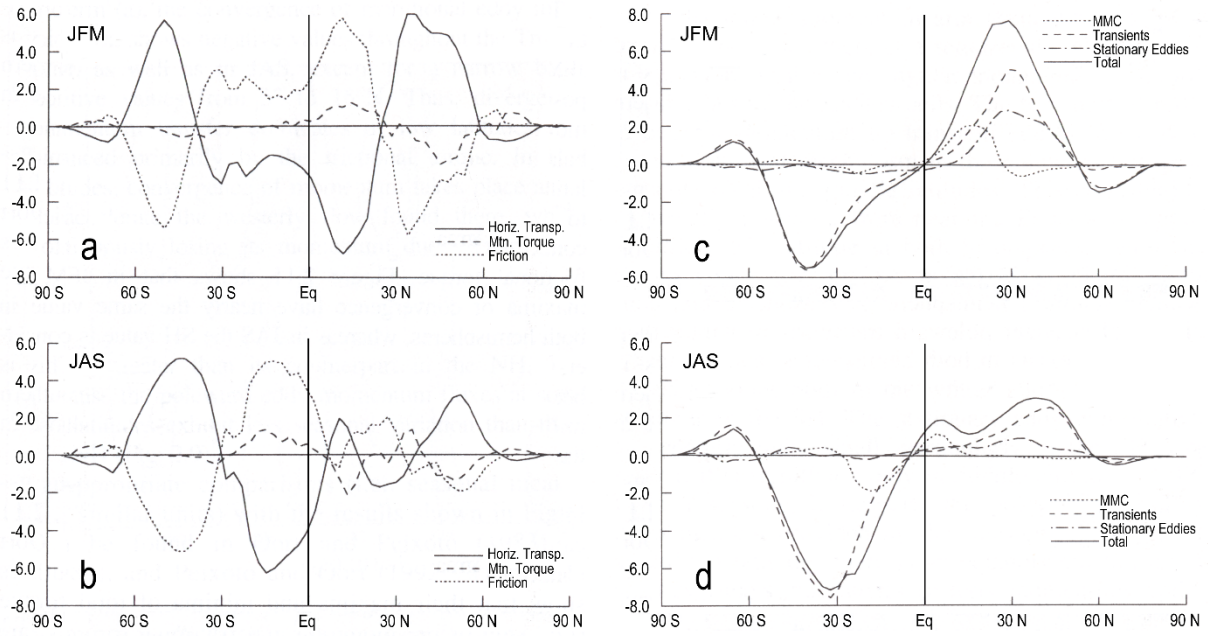

Figure 6.5 a),b)Terms from vertically-integrating the angular momentum equation per unit mass (6.13) in spherical geometry for unit latitude ranges. The solid line is from the meridional flux, positive when increasing zonal momentum. The dashed line is the topographic or mountain torque. The friction term (dotted line) is not explicitly calculated but estimated as a residual. a) January-March and b) July – September data from 1979-93. The units are 'Hadleys' (=10^{18} kg m^2 s^{-2}) per 2.5 degrees latitude. c), d) Corresponding seasonal contributors to the "Ruv" terms in (6.13) positive when directed northward; note that the meridional derivative of these terms is taken in the equation. In middle and subtropical latitudes the transients dominate, stationary eddies are strongest in NHem midlatitudes, and the MMC part is mainly from the winter hemisphere Hadley cell. The units are 10^{12} kg m s^{-2}. Redrawn from Karoly et al. (1998)

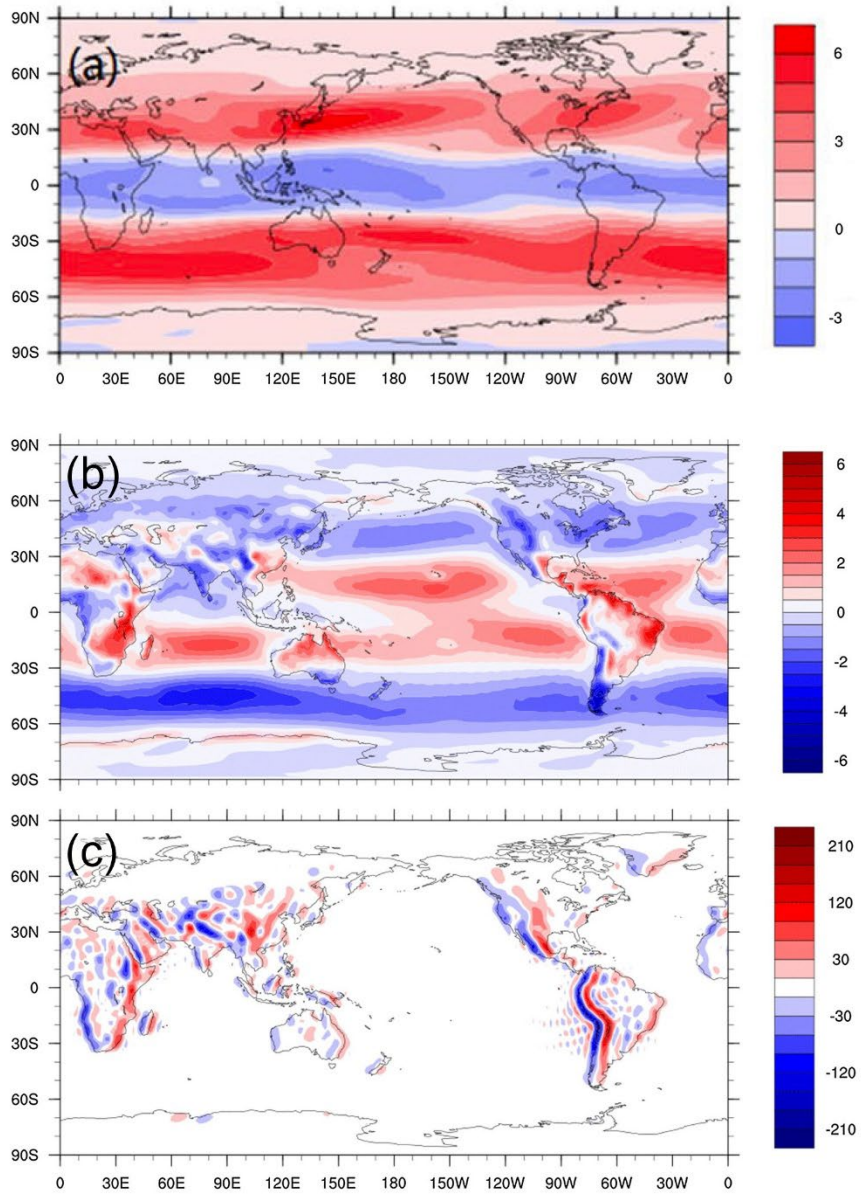

Figure 6.6 Horizontal variations of key parts of AAM. a) Vertically integrated long term mean "zonal wind part" of axial angular momentum, units: 10^{22} kg m^2 s^{-1}. This *annual* mean figure compares well with the *seasonal* mean horizontal winds in figure 4.14. Two torques in the AAM tendency equation: b) friction and c) mountain, with units 10^{22} kg m^2 s^{-2}. The friction torque has echoes of the zonal component of low-level wind vectors in figure 4.8. NCEP-NCAR reanalysis data from 1948-2015. Reproduced from Gong et al. (2019)

Need permission

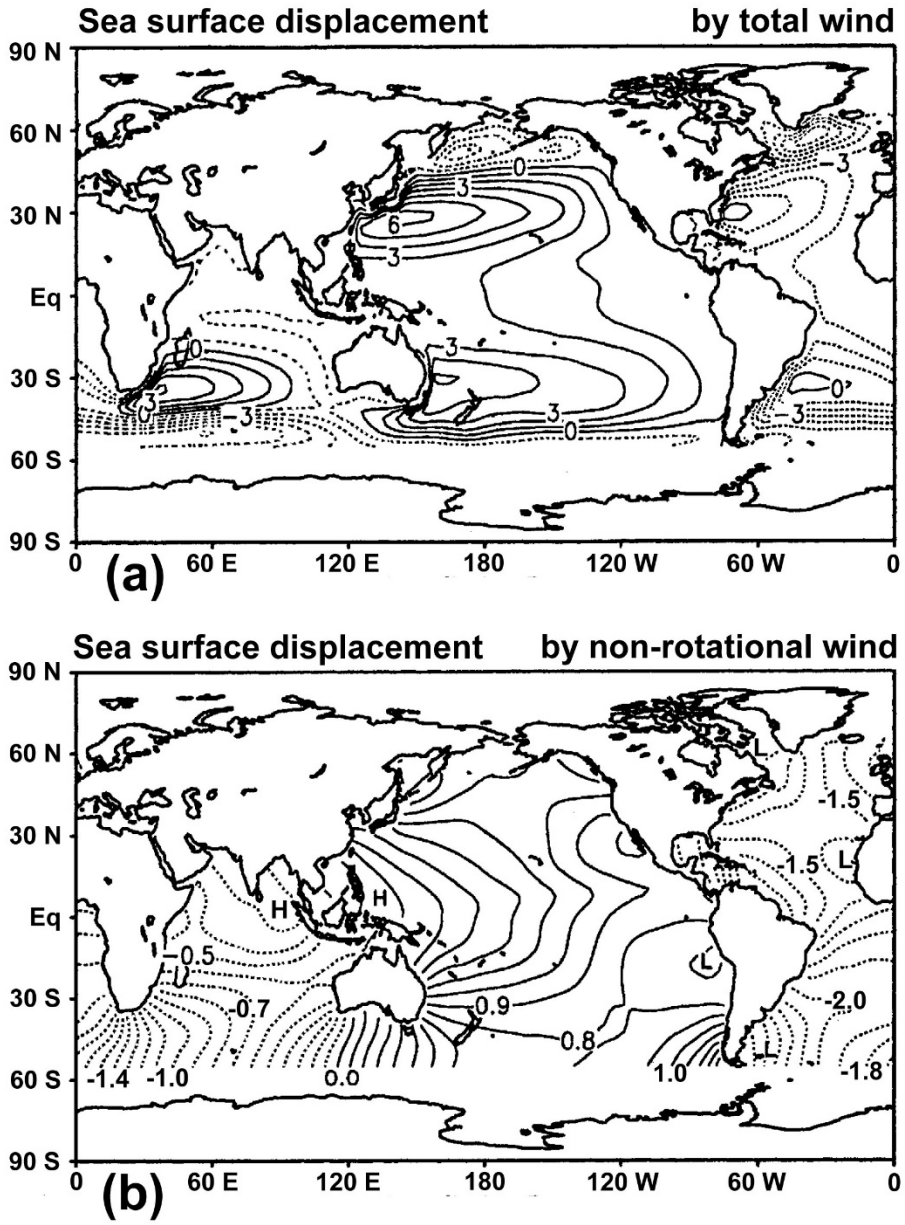

Figure 6.7 Simulated sea level displacements caused by realistic (a) total surface wind stress tensor and (b) non-rotational surface wind stress tensor. Contour interval differs: it is 10 mm in (a) and 1 mm in (b). Dotted lines indicate negative values. Redrawn from Yoshioka et al. (2002). Their model limitations exclude the Antarctic Circumpolar Current so the contours are not plotted south of 57.5 S. See the original reference for details.

Need Permission

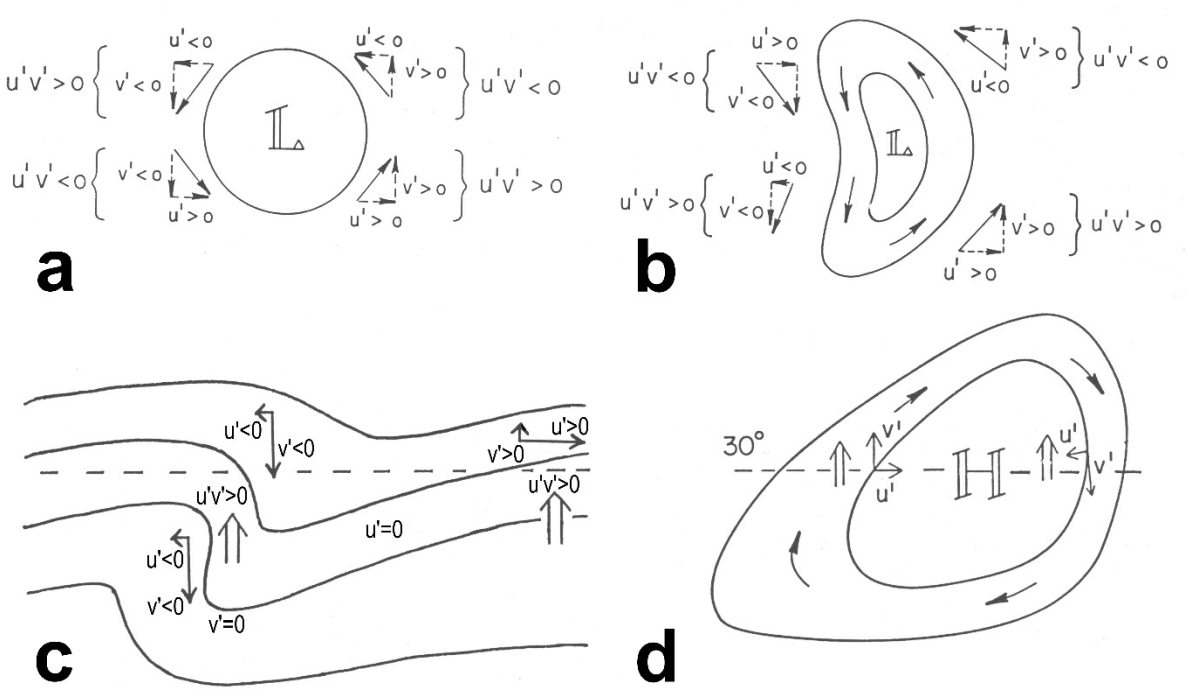

Figure 6.8 Schematic diagrams showing how geostrophic winds (thin arrows) around non-circular eddies can cause poleward $[u'v']$ fluxes (double-shafted arrows). Examples shown are as follows. (a) While there are momentum fluxes on both sides of a circular low, they cancel on a zonal average across that low. (b) A low with tilted horizontal troughs will have non-zero zonal average momentum fluxes and the direction of the flux depends on the orientation of the tilted troughs. (c) A schematic upper level tilted ridge and trough pair and northward motion embedded in a stronger zonal flow where both configurations produce positive $[u'v']$ flux. This combination occurs in the tropical north Atlantic across northern Africa in Figure 4.3a and 4.17a. (d) Surface subtropical high such as seen in the NHem of Figure 4.4c. (Panels revised from Grotjahn, 1993).

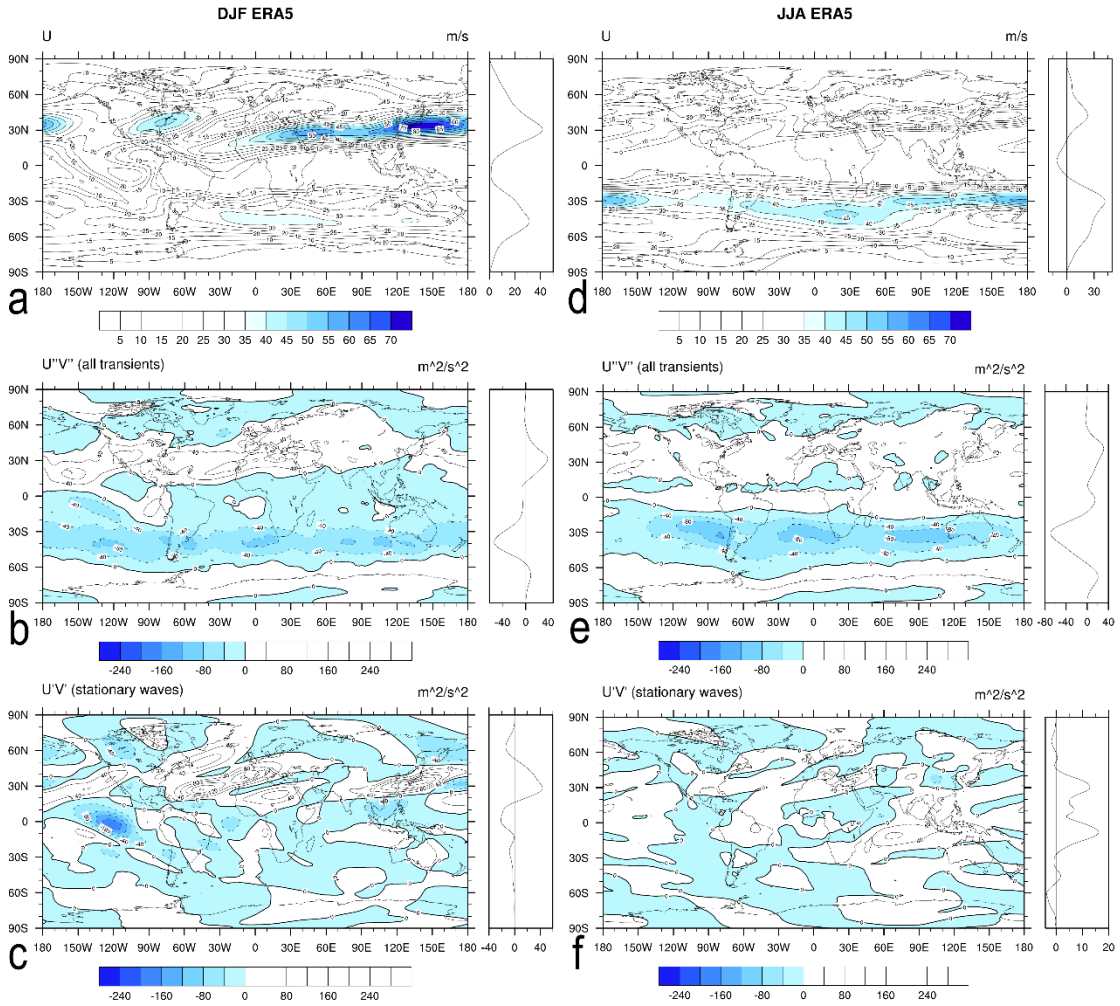

Figure 6.9 Zonal winds a) and b) and two parts of the meridional flux of zonal momentum at 200 hPa during DJF (left column) and JJA (right column) including the zonal average in right-side panels. b) and e) show time average $\overline{u''v''}$ while c) and f) show the contribution by stationary waves $\overline{u'}\,\overline{v'}$. Dashed contours indicate easterly flow in a) and d) with westerly winds >40 m/s shaded. Southward flux in the remaining panels is shaded. ERA5 data used are from 2001-2020. Contour interval is 5 m/s in a) and b); 40 m^2/s^2 in the other panels. The scale changes for the zonal means plotted in panels e) and f).

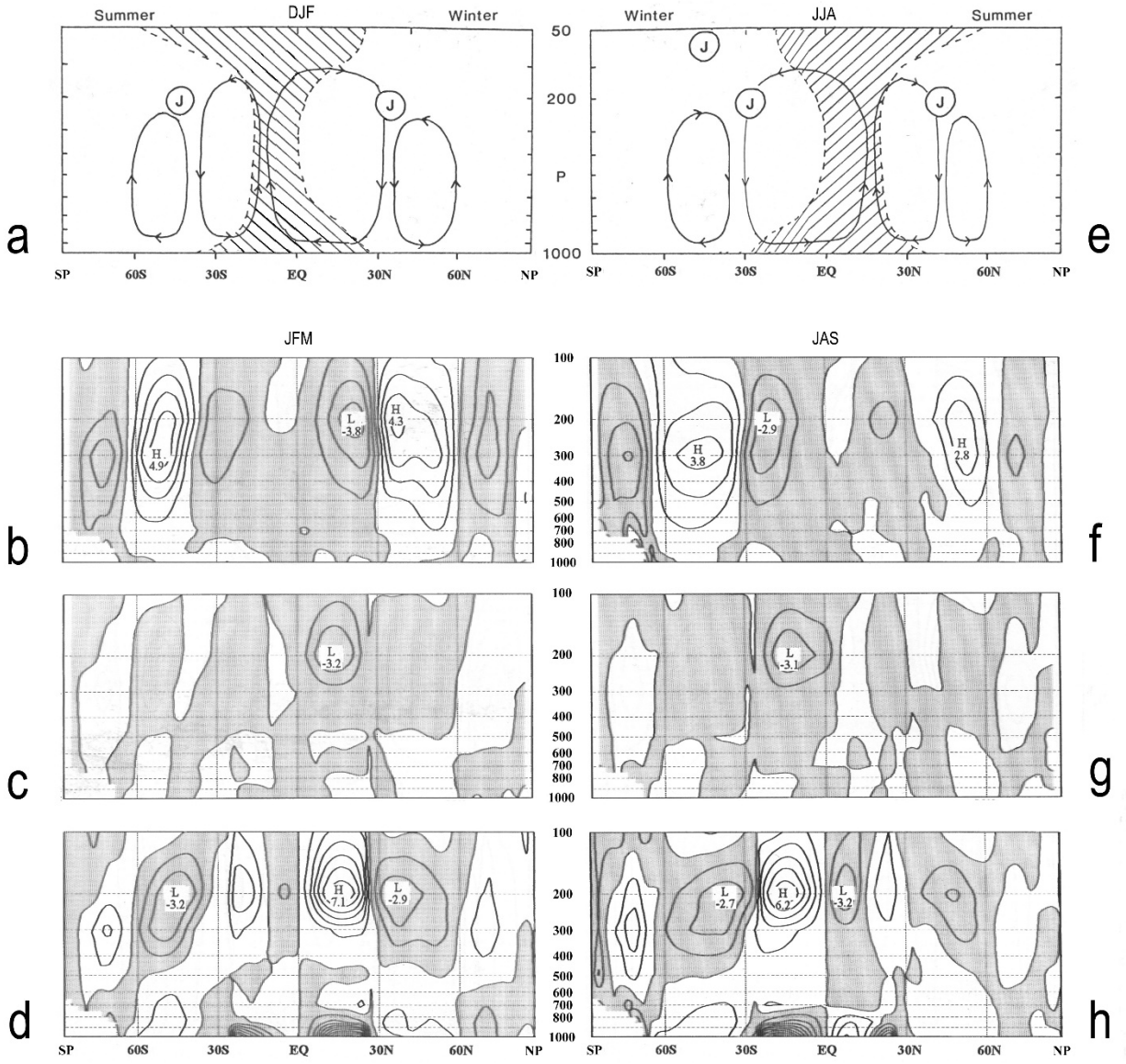

Figure 6.10 Key momentum balance terms in two opposite seasons. a) Schematic representation of the MMC and $[\bar{u}]$ during DJF based on figures 4.9 and 4.13. During related season JFM, selected terms in the $[\bar{u}]$ tendency equation: b) horizontal divergence of eddy horizontal velocity covariance, c) MMC advection of $[\bar{u}]$, d) (ageostrophic) Coriolis term. During the opposite season: e) as a) except for JJA, f)-h) as b)-d) except for JAS. Panels b-d and f-h are reproduced from Karoly et al. (1998). (need permission)